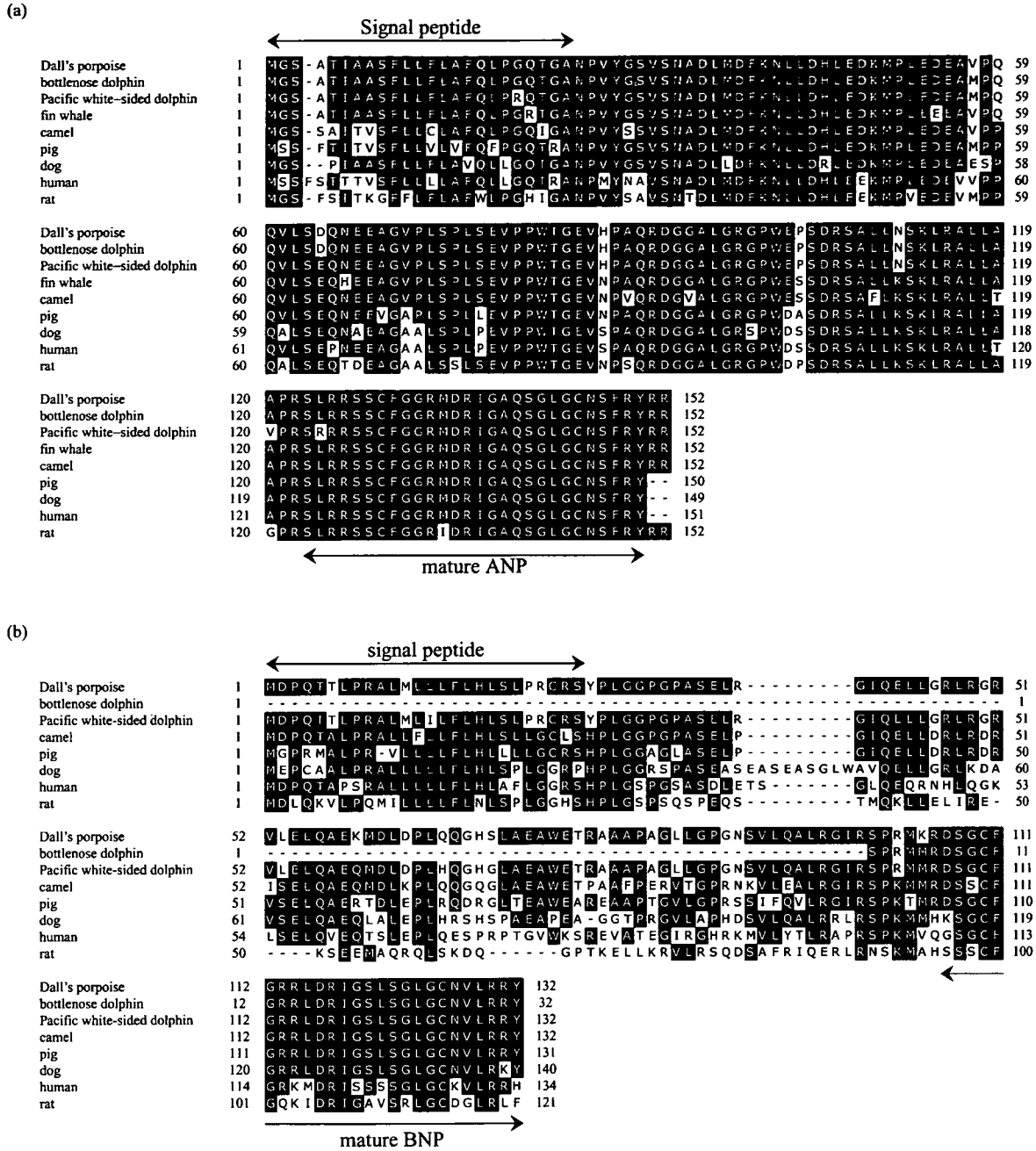

Fig. 1. Amino acid comparison of newly identified dolphin **(a)** ANP and **(b)** BNP precursor peptide sequences with those of other mammalian species. Identical amino acid residues in each group are shown in white-on-black. Accession numbers: Dall's porpoise ANP, AB284173; Dall's porpoise BNP, AB284169; bottlenose dolphin ANP, AB284172; bottlenose dolphin BNP, AB284170; Pacific white-sided dolphin ANP, AB284171; Pacific white-sided dolphin BNP, AB284168; fin whale ANP, AJ006785; camel ANP, AB127391; camel BNP, AB127392; pig ANP, X54669; pig BNP, M25547; dog ANP, AF484116; dog BNP, M31777; human ANP, M30262; human BNP, M31776; rat ANP, M27498; rat BNP, M25297.

deduced precursor sequences of ANP were highly conserved in mammals (>78%), whereas dolphin BNP precursors were much less conserved, with only 30% identity with that of mouse. The potential cleavage site for the signal peptide was deduced to follow Ala[24] for the ANP precursor and Ser[26] for the BNP precursor (Bendtsen *et al.*, 2004). The putative mature ANP may consist of 30 amino acid residues and two Arg residues at the C-terminal end that are removed by carboxyl peptidase, as judged from homology with other mammalian ANPs (Fig. 1a). Mature BNP is known to be cleaved by a proprotein convertase, furin, following the cleavage signal Arg/Lys-X-X-Arg (Seidah and Chretien, 1999). Hence, mature BNP may be cleaved off at the C-terminal end as a 32-amino-acid peptide, as shown for

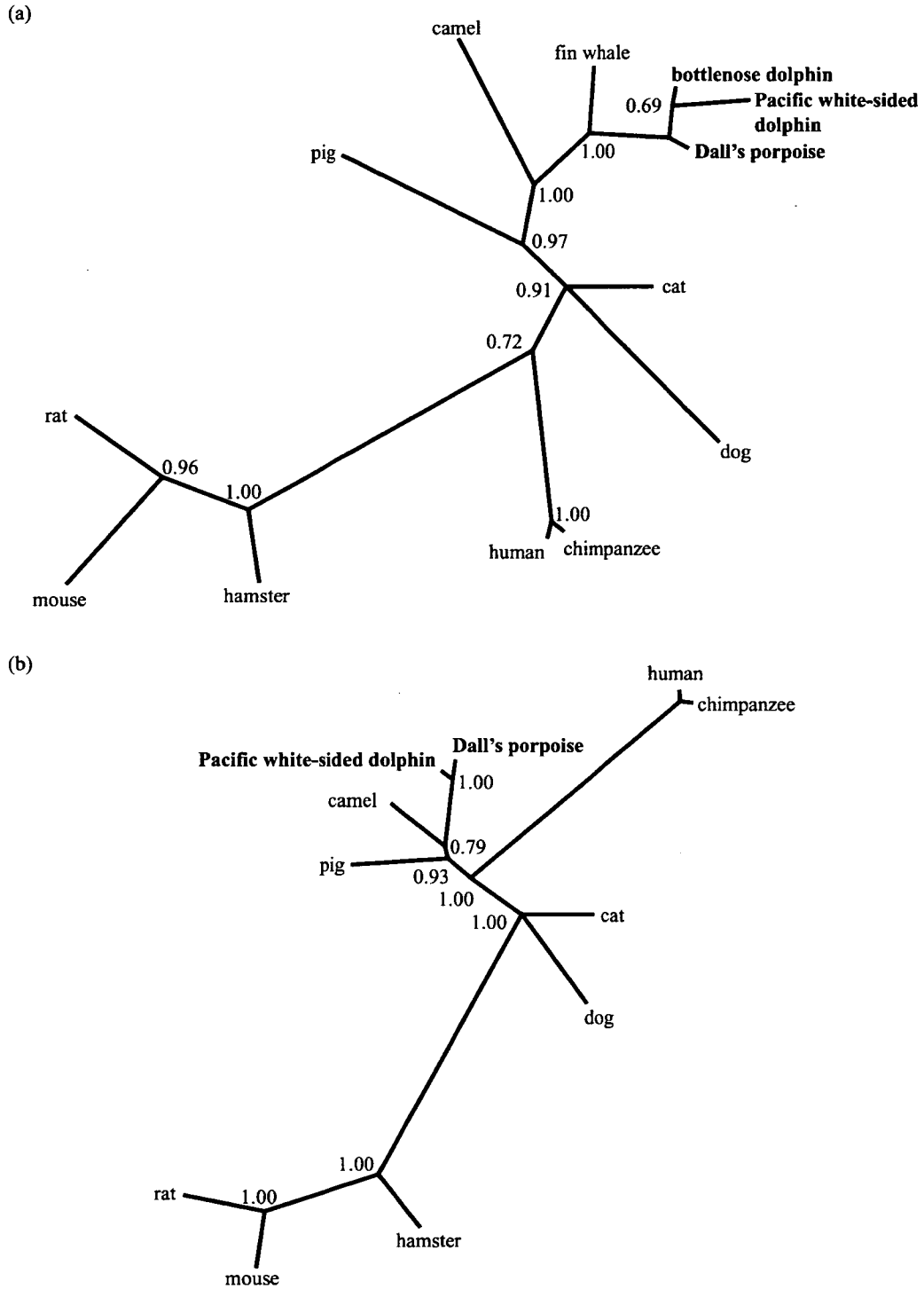

Fig. 2. Molecular phylogenetic trees of **(a)** ANP and **(b)** BNP from mammals, reconstructed from amino acid sequences of ANP and BNP precursors using the Bayesian method. The numbers near interior nodes are posterior probabilities. Accession numbers: cat ANP, AF298813; cat BNP, AF253495; chimpanzee ANP, XM_001141705; chimpanzee BNP, AB037522; mouse ANP, BC089615; mouse BNP, S58667; hamster ANP, D17313; hamster BNP, D17314.

humans (Nakayama *et al.*, 1992) or as a 26-amino-acid peptide as shown for the porcine brain (Fig. 1b).

Molecular phylogenetic analysis

In the molecular phylogenetic analysis using amino-acid sequences of ANP and BNP precursors, both NPs of cetaceans clustered near those of artiodactyls (Fig. 2). In particular, dolphin peptides were juxtaposed to those of camels. An analysis using nucleotide sequences produced similar results (data not shown).

Tissue distribution of ANP and BNP

The RT-PCR analyses showed that both ANP and BNP mRNAs are most abundantly expressed in the atrium (Fig. 3a). The expression of both genes was less in the ventricle than in the atrium. Expression was negligible in the kidney, but ANP expression was detected after an additional 5 cycles of PCR (Fig. 3a). BNP was expressed minutely in the kidney of one individual.

Immunoreactive ANP concentrations in the auricle, atrium, and ventricle were 3920.4±537.8, 2933.7±820.8, and 2.6±0.8 pmol/g·tissue (n=6), respectively. Immunoreactive BNP concentrations were 5.0±0.9, 3.0±0.5, and 0.2±0.01 pmol/g·tissue (n=6) in the auricle, atrium, and ventricle, respectively. The concentrations of immunoreactive ANP and BNP in the dolphin heart were much lower than in the heart of other mammalian species (Fig. 3b, c).

Molecular characterization

Fig. 4 shows the elution positions of immunoreactive ANP and BNP in reverse-phase and gel-permeation HPLC. ANP in the atrium eluted predominantly at a position more hydrophobic than that of mature ANP in reverse-phase HPLC. In subsequent separation by molecular mass using gel-permeation HPLC, ANP eluted at a void volume larger than 7 kDa. On the other hand, atrial BNP eluted at a position identical to BNP-26 in both reverse-phase and gel-permeation HPLC. Plasma ANP eluted as a single peak at the position of mature ANP-28. In contrast, plasma BNP immunoreactivity was spread over several peaks in the reverse-phase HPLC, corresponding to BNP-26 and other less hydrophobic peptides. However, since there are few

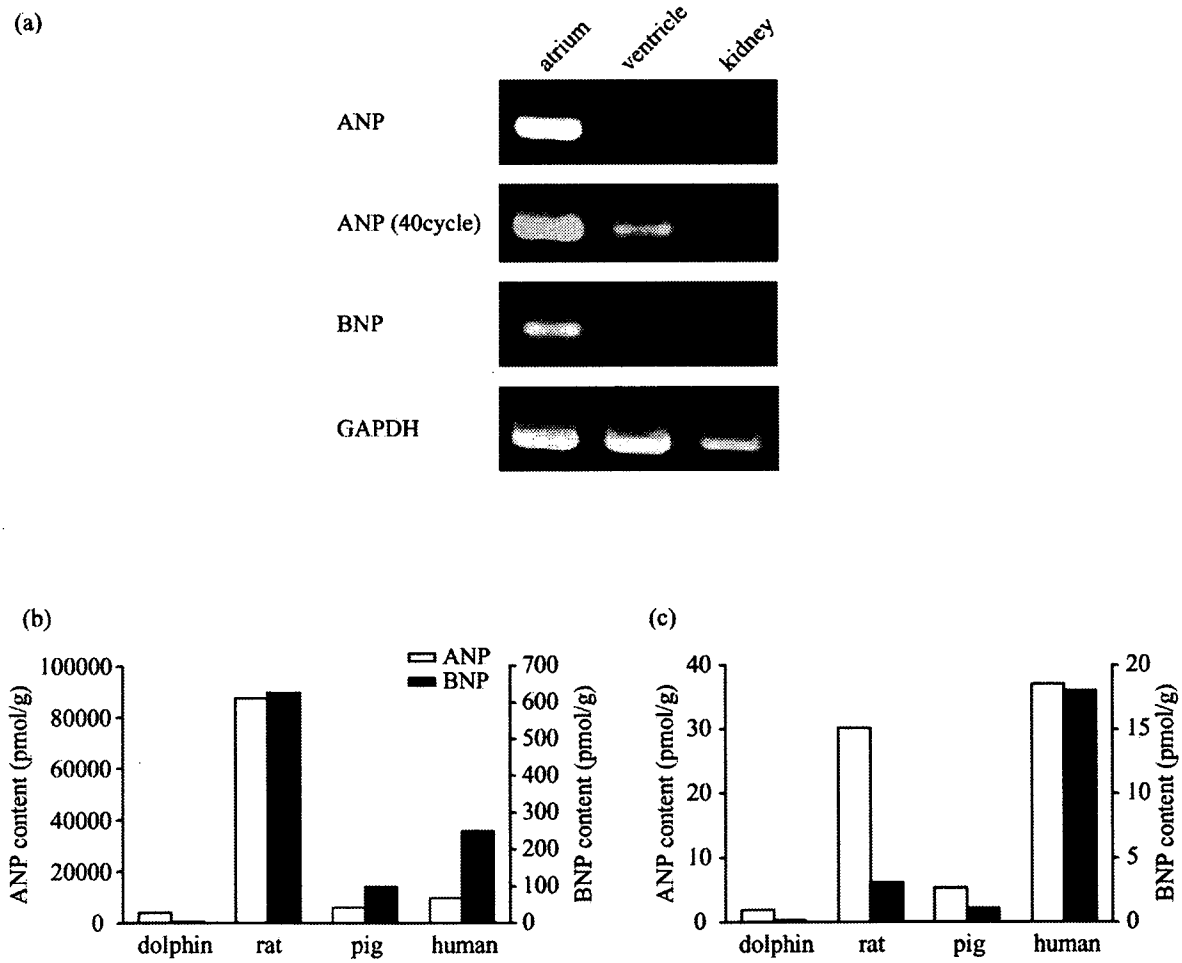

Fig. 3. **(a)** Tissue expression of ANP and BNP genes in the cardiac atrium, ventricle and kidney determined by RT-PCR. **(b)** Atrial (n=6) and (c) ventricular (n=6) immunoreactive ANP and BNP contents of bottlenose dolphin hearts compared to data from rat (Aburaya *et al.*, 1989b), human (Aburaya *et al.*, 1989c) and pig (Mukoyama *et al.*, 1991). Values are expressed as means.

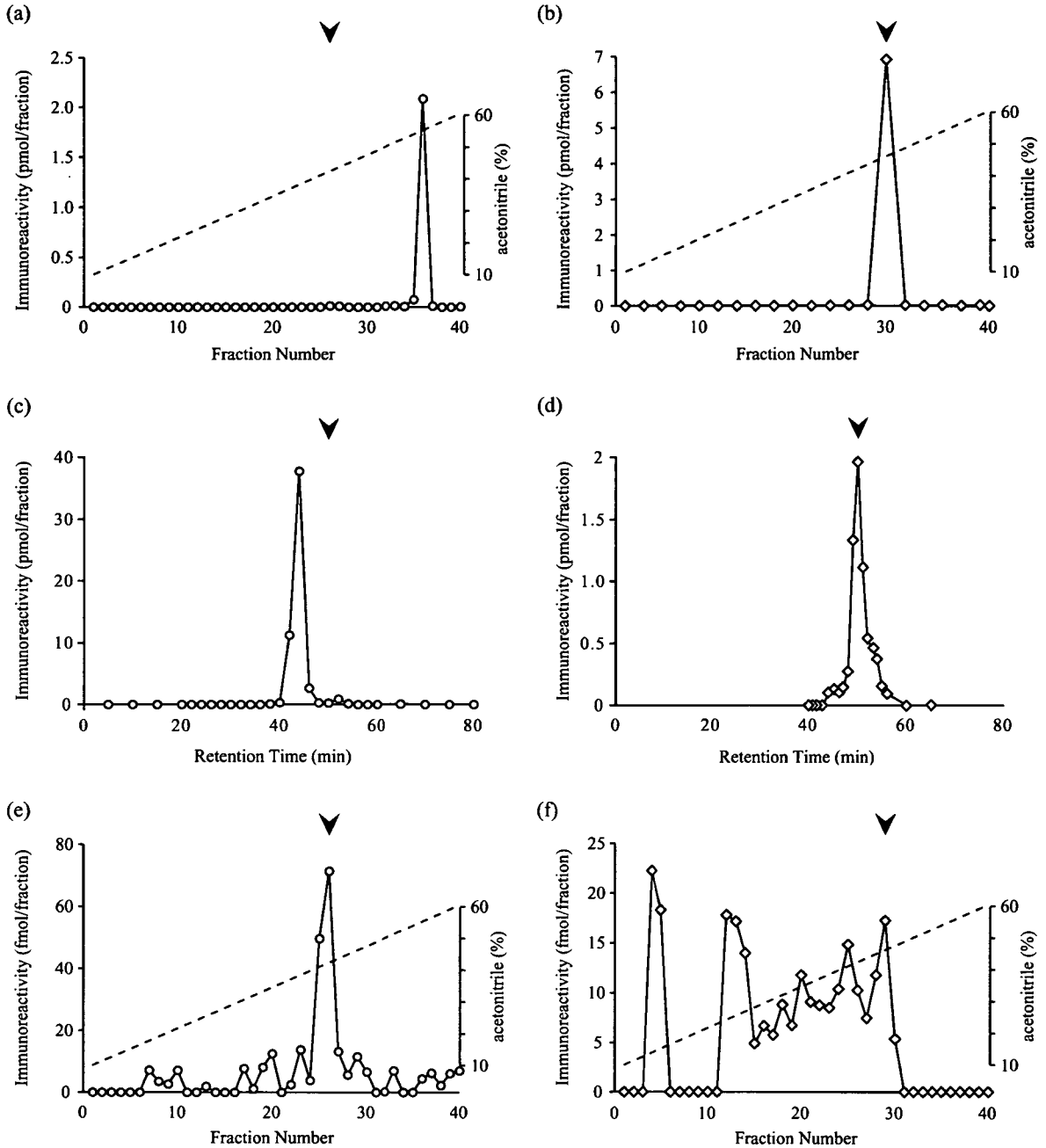

Fig. 4. Reverse-phase HPLC profiles of **(a)** atrial and **(b)** BNP; gel-permeation HPLC elution profiles of **(c)** atrial ANP and **(d)** BNP; and reverse-phase HPLC elution profiles of **(e)** plasma ANP and **(f)** BNP. Each symbol shows the amount of immunoreactive ANP or BNP. Arrows indicate elution positions of synthetic ANP-28 and BNP-26, respectively. Broken line shows the gradient of acetonitrile concentration.

amino-acid replacements in the putative mature sequence of dolphin BNP compared to the porcine peptide, the molecular form of atrial BNP cannot be determined only by the elution position in HPLC. The molecular mass of atrial BNP was determined by mass spectrometry. The theoretical molecular weights of putative mature BNP-32 (3625.2) and BNP-26 (2869.3) were calculated from deduced mature BNP sequences. The major mass signal was observed at an m/z value of 2868.5 and a small peak at 2930.5 in the SELDI mass spectrometry (Fig. 5). The latter peak may be a Na^+ and K^+ adduct of the m/z of 2868.5. This value was in good agreement with the theoretical molecular weight of BNP-26.

Gravitational experiment

Plasma concentrations of peptide and steroid hormones are shown in Table 2. In floating animals, the plasma ANP concentration was higher than that in humans (*e.g.*, 6.4±0.9 fmol/ml, n=6; Mukoyama *et al.*, 1991), and the value did not

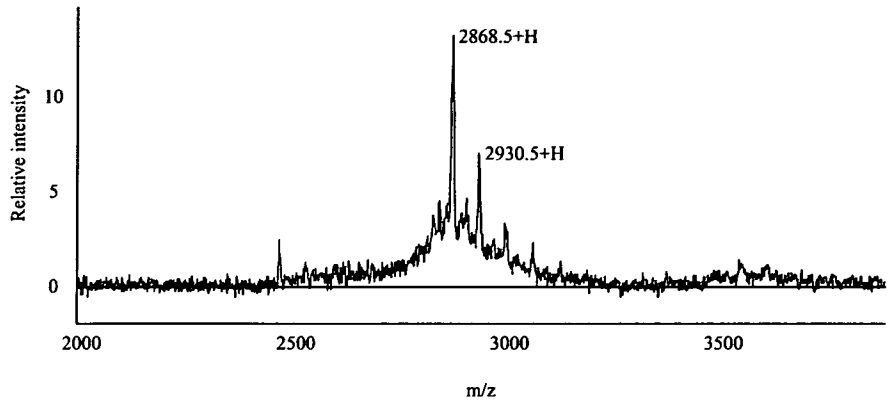

Fig. 5. Mass spectra of BNP-like materials in the dolphin atrium. The atrial materials were semipurified and subjected to immunoprecipitation.

Table 2. Plasma ANP, BNP, ANGII (fmol/ml) and cortisol concentration (ng/ml), and heart rate (beat.min), plasma osmolality (mmol/kg·H2O), ions and glucose concentrations (mM) in dolphins floating in water and after landed

	Floating	Landed
ANP	42.7±4.7	50.2±4.8
BNP	56.4±6.1	55.1±6.6
ANGII	46.3±6.8	61.5±8.9
Cortisol	3.7±1.1	10.6±1.3
Heart rate	60.2±4.6	75.3±3.9
Osmolality	330.1±3.4	327.3±1.5
Na^+	161.0±2.8	168.7±2.0
Cl^-	102.9±3.1	105.4±3.3
Glucose	4.6±0.3	4.8±0.3

change after landing. The plasma BNP concentration was also higher than in humans (0.9±0.07 fmol/ml, n=6; Mukoyama *et al.*, 1991), and the value did not change. Plasma ANGII and cortisol concentrations tended to increase after landing, but the increase was not significant. Heart rate could be measured in only three animals; landed animals showed an apparently higher value than floating animals, although the number of measurements was not sufficient to detect a significant difference. Plasma osmolality and Na^+, Cl^-, and glucose levels did not change after landing (Table 2).

DISCUSSION

Identification of ANP and BNP in cetaceans

In the present study, we identified ANP and BNP for the first time in marine mammals. The amino-acid sequences of dolphin ANP precursors are highly similar to those of other mammalian ANPs, while the dolphin BNP precursor does not show high similarity to other mammalian BNPs (Takei, 2000). The molecular phylogenetic analysis showed that the newly identified cetacean ANP and BNP precursors were close to those of artiodactyls, especially camels. A recent, detailed phylogenetic analysis of cetaceans suggested that the orders Cetacea and Artiodactyla should be combined into a new superorder, Cetartiodactyla (Price *et al.*, 2005). Our result using the precursor sequences of functional molecules provided additional support for this new classification.

Like marine cetaceans, camels are a highly adapted group of animals in terms of body-fluid regulation; they are desert dwellers and can survive long periods of desiccation under heat (Siebert and MacFarlane, 1975). Marine dolphins rarely have access to freshwater, and drinking seawater may cause severe dehydration due to the hypertonicity of seawater. It has been reported that cetaceans can concentrate urine hypertonic to seawater (Schmidt-Nielsen, 1997), but a recent report showed that several cetacean species caught in the wild have a urinary sodium concentration much lower than seawater (Birukawa *et al.*, 2005). Therefore, cetaceans may also produce metabolic water from stored fat to maintain water balance, as in camels. The close affinity of NP precursors between cetaceans and camels indicated in molecular phylogenetic trees might reflect their physiological function.

Molecular characterization of ANP and BNP

Dolphin ANP stored in the atrium in the form of prohormone consisted of 128 amino-acid residues, as is the case for other mammals (Miyata *et al.*, 1985). Only mature ANP-28 was detected in dolphin plasma, which suggests that proANP stored in the atrium is cleaved to form mature ANP at the time of secretion into the blood. In humans, mature ANP is cleaved from proANP following Arg at position 122 by the specific enzyme corin (Yan *et al.*, 2000). Since Arg^{122} is conserved in all cetacean ANP precursor sequences, a corin-like enzyme may also exist in cetaceans. The C-terminal two Arg residues may be removed by carboxyl peptidases immediately after cleavage. It is known that an antiparallel dimer of ANP-28 (β-ANP) is secreted from the failing human heart (Sugawara *et al.*, 1988), but it was not detectable in the tissue or plasma of the dolphins used in this study, suggesting that these animals may not have had any cardiac disorders.

Dolphin BNP stored in the atrium was determined by mass spectrometric analysis to be a C-terminal 26-amino-acid molecule, BNP-26. In other mammalian species, BNP-26 is known to exist only in the brain, where it was the first BNP identified in mammals (Sudoh *et al.*, 1988). In the heart, the predominant molecular form of BNP varies among species: proBNP in the pig (Minamino *et al.*, 1988), BNP-32 in humans (Hino *et al.*, 1990), and BNP-45 in rodents

(Aburaya *et al.*, 1989a). Differences in the mature form are due to the location of the processing signal in the prohormone sequence. In proBNP, the mature peptide is cleaved off following Arg/Lys-$(X)_n$-Arg (n=0, 2, 4, 6) (Seidah and Chretien, 1999). This signal is located 32 amino acids before the C-terminus in the dolphins, camel, pig, dog, and humans but is absent in rodents (Fig. 1). Instead, the mature rat BNP is cleaved at the Arg-Val-Leu-Arg sequence that exists 45 amino acids before the C-terminus. All dolphin BNP precursors have an additional Arg-X-X-Arg sequence after Pro^{102}, which might be cleaved by a furin-like enzyme after Arg^{106} and produce a 26-amino-acid BNP, as in artiodactyls such as the camel and pig. This difference explains why BNP-26 is produced as a mature peptide in these species, although proBNP can be detected as a major molecular form in the porcine heart.

The secretory pathway is different between ANP and BNP (Bloch *et al.*, 1986). ANP is stored in secretory granules in the heart and secreted into the blood in response to stimuli such as cardiac distension, which has been termed the 'regulatory pathway.' In contrast, BNP is principally secreted via the 'constitutive pathway,' in which newly synthesized hormones are immediately secreted without storage in granules. Therefore, it seems that ANP is stored as a prohormone in granules and secreted only in response to acute stimuli, whereas BNP is immediately processed into BNP-26 after translation and secreted continuously to maintain certain plasma levels.

Although BNP may be secreted from the heart in the form of BNP-26, various forms of BNP exists in dolphin plasma, as shown by the reverse-phase HPLC profiles. This may be due to the higher susceptibility to plasma peptidases and shorter half-life of BNP compared to ANP (Charles *et al.*, 1996). Shimizu *et al.* (2002) reported that BNP exists as the digested products of both proBNP and BNP-32 in the plasma of human patients with congestive heart failure. N- or C-terminal degradation of BNP in human plasma causes a large shift in retention time, to a more hydrophilic position. Shimizu *et al.* (2002) suggested that digestion might occur during circulation rather than after blood collection. Judging from the cross-reactivity, the antiserum used in this study recognizes the intra-molecular ring structure (Ueda *et al.*, 1988). Therefore, the plasma value measured in this study represents the endogenous BNP level, though considerable degradation occurred during circulation and handling after sampling.

Expression and concentration of ANP and BNP in tissues and plasma

Dolphin ANP and BNP mRNAs are more highly expressed in the atrium than in the ventricle. In the kidney, a trace amount of expression was detected for BNP but not ANP. In other mammals, the kidney synthesizes ANP and processes proANP into a different form, urodilatin (Bestle *et al.*, 1999). The role of ANP in the dolphin kidney might be negligible. It is of interest to examine the expression of ANP and BNP mRNAs in the brain, but we could not obtain fresh dolphin brain for this study.

The RIA system established in this study clearly recognized ANP and BNP in the dolphin heart and plasma. Immunoreactive ANP and BNP concentrations in the atrium and ventricle of Dall's porpoise were much lower than in terrestrial mammals (rat, Aburaya *et al.*, 1989b; pig, Aburaya *et al.*, 1989c; human, Mukoyama *et al.*, 1991). In contrast, the plasma concentrations of dolphin ANP and BNP were much higher than in terrestrial animals. Ding *et al.* (1987) reported that hamster hearts with artificially induced congestive heart failure show increased plasma ANP and decreased cardiac ANP concentrations. Thus, increased ANP secretion may account for the low cardiac content of proANP in dolphins. It has been reported that plasma ANP concentration increases in humans and dogs after head-out immersion in water (Shiraishi *et al.*, 2002; Sondeen *et al.*, 1990). This increased ANP secretion is caused by increased venous return to the heart and the resulting cardiac distension, due to the buoyancy of water counteracting the gravitational force that pulls the blood toward the ground. In this regard, head-out water immersion mimics space flight, which also induces an immediate increase in plasma ANP concentration (Leach *et al.*, 1988). Likewise, in a fetus surrounded by amniotic fluid, ANP is synthesized and secreted not only in the atrium but also in the ventricle, and fetal plasma concentrations are very high (Bloch *et al.*, 1986; Ito *et al.*, 1990). Cetaceans are thus also similar to the fetus, as both escape from the gravity.

Unlike ANP, the plasma BNP concentration does not change after head-out water immersion (Kurabayashi *et al.*, 2001). However, its plasma level is elevated by chronic volume or pressure loading to the heart, as occurs in congestive heart failure (Asano *et al.*, 1999). Since the gravity-free aquatic existence of dolphins chronically allows large venous return to the heart, it seems that the high plasma BNP levels are induced by a cardiac status resulting from total adaptation to an aquatic existence.

Changes in plasma hormone concentrations after landing

In terrestrial animals, head-out water immersion increases ANP secretion due to the increased venous return to the heart. Conversely, we expected that dolphins would decrease plasma ANP to the level of terrestrial mammals, which are exposed to gravitational force. However, plasma ANP concentrations in landed dolphins were no different from those in dolphins floating in the water. This result gives some indication of the involvement of cardiovascular status in ANP secretion in dolphins. The heart of dolphins is located in the ventral side of the body (Bossart *et al.*, 2001); hence, their heart may be compressed by their own weight, as is the case for humans in a prone position. In humans, the compressed heart cannot pump sufficient blood in a stroke, and the heart rate increases to compensate for the decreased stroke volume (Pump *et al.*, 2002). Increased heart rate is a major stimulus for ANP secretion (Lang *et al.*, 1985) and may have increased the plasma ANP level of landed dolphins to the level of floating ones. Kurabayashi *et al.* (2001) reported that plasma ANP and BNP levels of healthy humans significantly increase within 15 min after water immersion, so the time course of our experiment might have been sufficient to cause changes in cardiovascular status in the dolphins.

Similarly, the plasma BNP concentration did not change after the landing of dolphins. This was perhaps due to the

different secretory pathways of BNP and ANP mentioned above (Bloch *et al.*, 1986). It is known that the constitutive secretory pathway maintains plasma concentration at a certain level. This may be one reason why the plasma BNP concentration did not change after landing. Plasma cortisol concentration increases when animals are stressed (Thomson and Geraci, 1986), and cortisol is known to be involved in the expression of the ANP gene (Naruse *et al.*, 1987). However, plasma cortisol concentration did not change in this study after landing of the dolphins. The plasma cortisol levels of the captive bottlenose dolphins obtained in this study were similar to those of the same species in the wild reported by St. Aubin *et al.* (1996).

ACKNOWLEDGMENTS

We are grateful to Mr. Makoto Soichi, Mr. Kazutoshi Arai, and the staff of the Marine Mammal Section of Kamogawa Sea World for animal experiments, and to Dr. Masao Amano of Teikyo University of Science and Technology, Mr. Koji Tokutake of Yokohama Hakkeijima Sea Paradise, and Mr. Masayuki Nakamura of Marine World Uminonakamichi for the collection of tissue samples. We also thank Dr. Mitsuhide Naruse of Tokyo Women's Medical University for the generous gift of ANP antisera; and Dr. Sinya Yuge of University of Missouri-Columbia, and Dr. Susumu Hyodo and Ms. Sanae Hasegawa of the Ocean Research Institute, for technical assistance and valuable discussions. This work was supported by a Grant-in-Aid for Basic Research (A) from Japan Society for the Promotion of Science to YT (16207004), and a Creative Basic Research grant from the Ministry of Education, Culture, Sports, Science, and Technology of Japan (12NP0201).

REFERENCES

Aburaya M, Hino J, Minamino N, Kangawa K, Matsuo H (1989a) Isolation and identification of rat brain natriuretic peptides in cardiac atrium. Biochem Biophys Res Commun163: 226–232

Aburaya M, Minamino N, Hino J, Kangawa K, Matsuo H (1989b) Distribution and molecular forms of brain natriuretic peptide in the central nervous system, heart and peripheral tissue of rat. Biochem Biophys Res Commun 165: 880–887

Aburaya M, Minamino N, Kangawa K, Tanaka K, Matsuo H (1989c) Distribution and molecular forms of brain natriuretic peptide in porcine heart and blood. Biochem Biophys Res Commun 165: 872-879

Asano K, Masuda K, Okumura M, Kadosawa T, Fujinaga T (1999) Plasma Atrial and brain natriuretic peptide levels in dogs with congestive heart failure. J Vet Med Sci 61: 523–529

Bendtsen JD, Nielsen H, Heijne GV, Brunak S (2004) Improved prediction of signal peptides: SignalP 3.0. J Mol Biol 340: 783–795

Bestle MH, Olsen NV, Christensen P, Jensen BV, Bie P (1999) Cardiovascular, endocrine, and renal effects of urodilatin in normal humans. Am J Physiol 276: R684–695

Birukawa N, Ando H, Goto M, Kanda N, Pastene LA, Nakatsuji H, Hata H, Urano A (2005) Plasma and urine levels of electrolytes, urea and steroid hormones involved in osmoregulation of cetaceans. Zool Sci 22: 1245–1257

Bloch KD, Seidman JG, Naftilan JD, Fallon JT, Seidman CE (1986) Neonatal atria and ventricles secrete atrial natriuretic factor via tissue-specific secretory pathways. Cell 47: 695–702

Bossart GD, Reidarson TH, Dierauf LA, Duffield DA (2001) Clinical Pathology. In "CRC Handbook of Marine Mammal Medicine" 2nd ed Ed by LA Dierauf, FMD Gulland, CRC Press, New York, pp 383–436

Charles CJ, Espiner EA, Richards AM, Nicholls MG, Yandle TG (1996) Comparative bioactivity of atrial, brain, and C-type natriuretic peptides in conscious sheep. Am J Physiol 270: R1324–1331

Clerico A, Recchia FA, Passino C, Emdin M (2006) Cardiac endocrine function is an essential component of the homeostatic regulation network: physiological and clinical implications. Am J Physiol 290: H17–29

Ding J, Thibault G, Gutkowska J, Garcia R, Karabatsos T, Jasmin G, Genest J, Cantin M (1987) Cardiac and plasma atrial natriuretic factor in experimental congestive heart failure. Endocrinol 12: 248–257

Elsner R, Kenney DW, Burgess K (1966) Diving bradycardia in the trained dolphin. Nature 212: 407–408

Hino J, Tateyama H, Minamino N, Kangawa K, Matsuo H (1990) Isolation and identification of human brain natriuretic peptides in cardiac atrium. Biochem Biophys Res Commun 167: 693–700

Ito Y, Marumo F, Ando K, Hayashi M, Yamashita F (1990) The physiological and biological significances of human atrial natriuretic peptide in neonates. Acta Paediatr Scand 79: 26–31

Jones DT, Taylor WR, Thornton JM (1992) The rapid generation of mutation data matrices from protein sequences. Comput Appl Biosci 8: 275–282

Kaiya H, Takei Y (1996) Atrial and ventricular natriuretic peptide concentrations in plasma of freshwater- and seawater-adapted eels. Gen Comp Endocrinol 102: 183–190

Kikuchi K, Nakao K, Hayashi K, Morii N, Sugawara A, Sakamoto M, Imura H, Mikawa H (1987) Ontogeny of atrial natriuretic polypeptide in the human heart. Acta Endocrinol 115: 211–217

Kurabayashi H, Tamura K, Tamura J, Kubota K (2001) The effects of hydraulic pressure on atrial natriuretic peptide during rehabilitative headout water immersion. Life Sci 69: 1017–1021

Lang RE, Thölken H, Ganten D, Luft FC, Ruskoaho H, Unger T (1985) Atrial natriuretic factor — a circulating hormone stimulated by volume loading. Nature 314: 264–266

Leach CS, Johnson PC, Cintron NM (1988) The endocrine system in space flight. Acta Astronaut 17: 161–166

Mantymaa P, Vuolteenaho O, Marttila M, Ruskoaho H (1992) Atrial stretch induces rapid increase in brain natriuretic peptide but not in atrial natriuretic peptide gene expression *in vitro*. Endocrinology 133: 1474–1477

Minamino N, Aburaya M, Ueda S, Kangawa K, Matsuo M (1988) The presence of brain natriuretic peptide of 12000 daltons in porcine heart. Biochem Biophys Res Commun 155: 740–746

Miyata A, Kangawa K, Toshimori T, Hatoh T, Matsuo H (1985) Molecular forms of atrial natriuretic polypeptides in mammalian tissues and plasma. Biochem Biophys Res Commun 129: 248–255

Mukoyama M, Nakao K, Hosoda K, Suga S, Saito Y, Ogawa Y, Shirakami G, Jougasaki M, Obata K, Yasue H, Kambayashi Y, Inouye K, Imura H (1991) Brain natriuretic peptide as a novel cardiac hormone in human. J Clin Invest 87: 1402–1412

Naruse M, Obata K, Narse K, Yamaguchi H, Demura H, Inagami T, Shizume K (1987) Atrial natriuretic polypeptide inhibits cortisol secretion as well as aldosterone secretion *in vitro* from human adrenal tissue. J Clin Endocrinol Metab 64: 10–16

Price SA, Bininda-Emonds ORP, Gittleman JL (2005) A complete phylogeny of the whales, dolphins and even-toed hoofed mammals (Cetartiodactyla). Biol Rev 80: 445–473

Pump B, Talleruphuus U, Christensen NJ, Warberg J, Norsk P (2002) Effects of supine, prone, and lateral positions on cardiovascular and renal variables in humans. Am J Physiol 283: R174–180

Ronquist F, Huelsenbeck JP (2003) MrBayes 3: Bayesian phylogenetic inference under mixed models. Bioinformatics 19: 1572–1574

Sasaki K, Sato K, Akiyama Y, Yanagihara K, Oka M, Yamaguchi K (2002) Peptidomics-based approach reveals the secretion of the 29-residue COOH-terminal fragment of the putative tumor suppressor protein DMBT1 from pancreatic adenocarcinoma

cell lines. Cancer Res 62: 4894–4898
Schmidt-Nielsen K (1997) Water and osmotic regulation. In "Animal Physiology: Adaptation and Environment," 5th ed, Cambridge University Press, Cambridge, pp 301–354
Seidah NG, Chretien M (1999) Proprotein and prohormone convertases: a family of subtilases generating diverse bioactive polypeptides. Brain Res 848: 45–62
Shimizu H, Masuta K, Aono K, Asada H, Sasakura K, Tamaki M, Sugita K, Yamada K (2002) Molecular forms of human brain natriuretic peptide in plasma. Clin Chim Acta 316: 129–135
Shiraishi M, Schou M, Gybel M, Christensen NJ, Norsk P (2002) Comparison of acute cardiovascular responses to water immersion and headdown tilt in humans. J Appl Physiol 92: 264–268
Siebert BD, MacFarlane WV (1975) Dehydration in desert cattle and camels. Physiol Zool 48: 36–48
Sondeen JL, Hong SK, Claybauch JR, Krasney JA (1990) Effect of hydration state on renal responses to head-out water immersion in conscious dogs. Undersea Biomed Res 17: 395–411
St. Aubin DJ, Ridgway SH, Wells RS, Rhinehart H (1996) Dolphin thyroid and adrenal hormones: circulating levels in wild and semidomesticated *Tursiops truncatus*, and influence of sex, age, and season. Mar Mamm Sci 12: 1–13
Sudoh T, Kangawa K, Minamino N, Matsuo H (1988) A new natriuretic peptide in porcine brain. Nature 332: 78–81
Sugawara A, Nakao K, Morii N, Yamada T, Itoh H, Shiono S, Saito Y, Mukoyama M, Arai H, Nishimura K, Obata K, Yasue H, Ban T, Imura H (1988) Augmented synthesis of β-human atrial natriuretic peptide in human failing hearts. Biochem Biophys Res Commun 150: 60–67
Takei Y (2000) Structural and functional evolution of the natriuretic peptide system in vertebrates. Int Rev Cytol 194: 1–66
Takei Y, Takahashi A, Watanabe TX, Nakajima K (1989) Amino acid sequence and relative biological activity of eel atrial natriuretic peptide. Biochem Biophys Res Commun 164: 537–543
Takei Y, Inoue K, Ando K, Ihara T, Katafuchi T, Kashiwagi M, Hirose S (2001) Enhanced expression and release of C-type natriuretic peptide in freshwater eels. Am J Physiol 280: R1727–735
Thomson CA, Geraci JR (1986) Cortisol, aldosterone, and leucocytes in the stress response of bottlenose dolphins, *Tursiops truncatus*. Can J Fish Aquat Sci 43: 1010–1016
Tsuchida T, Takei Y(1998) Effects of homologous atrial natriuretic peptide on drinking and plasma ANG II level in eels. Am J Physiol 275: R1605–1610
Ueda S, Minamino N, Sudoh T, Kangawa K, Matsuo H (1988) Regional distribution of immunoreactive brain natriuretic peptide in porcine brain and spinal cord. Biochem Biophys Res Commun 155: 733–739
Yan W, Wu F, Morser J, Wu Q (2000) Corin, a transmembrane cardiac serine protease, acts as a pro-atrial natriuretic peptide-converting enzyme. Proc Natl Acad Sci USA 97: 8525–8529
Zenteno-Savin T, Castellini MA (1998a) Plasma angiotensin II, arginine vasopressin and atrial natriuretic peptide in free ranging and captive seals and sea lions. Comp Biochem Physiol 119: 1–6
Zenteno-Savin T, Castellini MA (1998b) Changes in the plasma levels of vasoactive hormones during apnea in seals. Comp Biochem Physiol 119: 7–12

(Received November 25, 2006 / Accepted January 2, 2007)

THE JOURNAL OF BIOLOGICAL CHEMISTRY VOL. 282, NO. 36, pp. 26354–26360, September 7, 2007

Peptidomic Identification and Biological Validation of Neuroendocrine Regulatory Peptide-1 and -2*

Received for publication, February 26, 2007, and in revised form, June 25, 2007 Published, JBC Papers in Press, July 3, 2007, DOI 10.1074/jbc.M701665200

Hideki Yamaguchi[‡1], Kazuki Sasaki[§1], Yoshinori Satomi[¶1], Takuya Shimbara[‡], Haruaki Kageyama[‖], Muhtashan S. Mondal[‡], Koji Toshinai[‡], Yukari Date[‡], Luis J. González[**], Seiji Shioda[‖], Toshifumi Takao[¶], Masamitsu Nakazato[‡2], and Naoto Minamino[§3]

From the [‡]Division of Neurology, Respirology, Endocrinology, and Metabolism, Department of Internal Medicine, Miyazaki Medical College, University of Miyazaki, Kihara, Kiyotake, Miyazaki 889-1692, Japan, the [§]Department of Pharmacology, National Cardiovascular Center Research Institute, Fujishirodai, Suita, Osaka 565-8565, Japan, [¶]Laboratory of Protein Profiling and Functional Proteomics, Institute for Protein Research, Osaka University, Yamadaoka, Suita, Osaka 565-0871, Japan, [‖]Department of Anatomy, Showa University School of Medicine, Hatanodai, Shinagawa-ku, Tokyo 142-8555, Japan, and [**]Physical-Chemistry Division, Center for Genetic Engineering and Biotechnology, P. O. Box 6162, Havana, Cuba

Recent advances in peptidomics have enabled the identification of previously uncharacterized peptides. However, sequence information alone does not allow us to identify candidates for bioactive peptides. To increase an opportunity to discover bioactive peptides, we have focused on C-terminal amidation, a post-translational modification shared by many bioactive peptides. We analyzed peptides secreted from human medullary thyroid carcinoma TT cells that produce amidated peptides, and we identified two novel amidated peptides, designated neuroendocrine regulatory peptide (NERP)-1 and NERP-2. NERPs are derived from distinct regions of the neurosecretory protein that was originally identified as a product of a nerve growth factor-responsive gene in PC12 cells. Mass spectrometric analysis of the immunoprecipitate using specific antibodies as well as reversed phase-high performance liquid chromatography coupled with radioimmunoassay analysis of brain extract demonstrated the endogenous presence of NERP-1 and NERP-2 in the rat. NERPs are abundant in the paraventricular and supraoptic nuclei of the rat hypothalamus and colocalized frequently with vasopressin but rarely with oxytocin. NERPs dose-dependently suppressed vasopressin release induced by intracerebroventricular injection of hypertonic NaCl or angiotensin II *in vivo*. NERPs also suppressed basal and angiotensin II-induced vasopressin secretion from hypothalamic explants *in vitro*. Bioactivity of NERPs required C-terminal amidation. Anti-NERP IgGs canceled plasma vasopressin reduction in response to water loading, indicating that NERPs could be potent endogenous suppressors of vasopressin release. These findings suggest that NERPs are novel modulators in body fluid homeostasis.

* This work was supported in part by the 21st Century COE Program of the Ministry of Education, Culture, Sports, Science, and Technology (to M. N.), Takeda Science Foundation (to H. Y.), and the Program for Promotion of Fundamental Studies in Health Sciences of the National Institute of Biomedical Innovation (to N. M.) of Japan. The costs of publication of this article were defrayed in part by the payment of page charges. This article must therefore be hereby marked "*advertisement*" in accordance with 18 U.S.C. Section 1734 solely to indicate this fact.

[1] These authors contributed equally to this work.
[2] To whom correspondence may be addressed. Tel.: 81-985-85-2965; Fax: 81-985-85-1869; E-mail: nakazato@med.miyazaki-u.ac.jp.
[3] To whom correspondence may be addressed. Tel.: 81-6-6833-5012; Fax: 81-6-6835-5349; E-mail: minamino@ri.ncvc.go.jp.

Peptide hormones or neuropeptides function as cell-to-cell signaling molecules to mediate a variety of physiological phenomena. These bioactive peptides are cleaved from precursor proteins via limited cleavage and often undergo post-translational modifications to perform their functions (1). Technological advancement in mass spectrometry, along with an ever increasing number of genomes being sequenced, has made it possible to study the peptidome or a whole set of endogenously processed peptides. In fact, peptidomic approaches have been applied to the analysis of peptides found in mammalian tissues or body fluids, leading to the description of a number of previously uncharacterized peptides (2–4).

In mammalian peptidomic studies, however, most peptides identified are fragments of intracellular proteins. Even in the studies designed to identify pituitary and hypothalamic peptides using specific sample preparation methods (5, 6), the peptides identified have turned out to be N-terminally or C-terminally deleted or extended fragments of relatively abundant precursors of known peptide hormones or secretory proteins. This is because mass spectrometry schemes detect only abundant molecules or easily ionized molecules, although tandem mass spectrometry has the potential to efficiently identify peptides present in complex mixtures. Thus, candidates for novel bioactive peptides present in trace amounts remain elusive in peptidomic identification studies. Another critical issue in peptidomics is that we cannot infer biological activity just from the sequence of a target peptide; it is practically impossible to synthesize and test all the peptidomic-identified peptides for assessing bioactivity.

We thought that one solution to increase the probability of identifying potentially bioactive peptides is to focus on secretory peptides with a post-translational modification characteristic of bioactive peptides. In this study, we targeted C-terminal amidation, which is shared by many known bioactive peptides or peptide hormones (7). By analyzing peptides released by a human cell line of endocrine origin, we discovered two C-terminally amidated peptides derived from the neurosecretory protein VGF (8). Although VGF has long been considered a precursor of bioactive peptides, functional studies are limited to C-terminal peptides as yet (9, 10). Biological functions of other VGF-related peptides, identified by recent peptidomic

studies, have not been investigated (11, 12). To get a clue for identifying their biological functions, we prepared antisera against these peptides and performed immunohistochemical studies to identify peptide-producing tissues and cells in the rat. We took advantage of the well documented findings on the localization and production sites of peptide hormones and deduced the possible biological functions of candidate peptides in relation to these known peptide hormones. This study would provide a new approach to the peptidomics-aided discovery of mammalian bioactive peptides.

EXPERIMENTAL PROCEDURES

Mass Spectrometric Analysis—The supernatant of human medullary thyroid carcinoma TT cells (13) cultured in serum-free media for 6 h was harvested and immediately processed using a Sep-Pak C18 cartridge (Waters) as described (14). The resultant eluate was applied to a gel filtration column (Superdex Peptide PE7.5/300, GE Healthcare) to obtain peptide-rich fractions. These were subjected to reductive alkylation, desalted, and fractionated by RP-HPLC[4] into 50 fractions. Each fraction was analyzed by off-line nano-electrospray ionization MS/MS with a Q-Tof II mass spectrometer (Micromass, Milford, MA) and by matrix-assisted laser desorption ionization-time of flight MS/MS with a Proteomics 4700 mass spectrometer (Applied Biosystems, Foster City, CA). Each MS/MS spectrum was used to probe the NCBI and Swiss-Prot databases with Mascot MS/MS ion search software (Matrix Science, Boston, MA) and was also interpreted by SeqMS (15).

Peptide Synthesis—All peptides were synthesized on an Abacus peptide synthesizer (Sigma Genosys) using Fmoc (*N*-(9-fluorenyl) methoxycarbonyl) strategy, purified by RP-HPLC, and verified for correct synthesis by mass spectrometry and amino acid analysis. Purity of the peptides was confirmed on separate HPLC systems. Synthetic rat NERPs were used in all the *in vivo* and *in vitro* administration experiments.

Antibody Preparation and Radioimmunoassay (RIA)—A C-terminal octapeptide common to human and rat NERP-1 (QGLAQVEA-NH_2) was conjugated with keyhole limpet hemocyanin (Pierce) by the glutaraldehyde method. Cysteinyl C-terminal decapeptides of rat NERP-2 (CQGGARQRDLG-NH_2) and human NERP-2 (CQGGARQRGLG-NH_2) were each coupled with maleimide-activated keyhole limpet hemocyanin (Pierce) through its thiol groups. Rabbits were immunized with each conjugate emulsified with an equal volume of Freund's complete adjuvant. Radioimmunoassay was carried out as reported (16) using ^{125}I-radiolabeled YLLQQGLAQVEA-NH_2 (human and rat NERP-1), YLLQGGARQRDLG-NH_2 (rat NERP-2), or YQGGARQRGLG-NH_2 (human NERP-2). A half-maximum inhibition concentration of ligand binding in each RIA was 20 fmol/tube (human and rat NERP-1), 10 fmol/tube (rat NERP-2), or 20 fmol/tube (human NERP-2). Specificity of the three RIAs for human/rat NERP-1 and rat NERP-2 was examined with immunized peptides with C-terminal Gly extension, C-terminal rat VGF-(588–617) and human VGF-(586–615), rat VGF-(556–585), and human VGF-(554–583) corresponding to a C-terminally extended form of TLQP-21 (10) and 13 known bioactive peptides listed below, including 10 C-terminally amidated peptides. Vasopressin, neuromedin U, neurokinin A, calcitonin, calcitonin gene-related peptide, calcitonin receptor-stimulating peptide, adrenomedullin, proadrenomedullin N-terminal 20-amino acid peptide, peptide histidine isoleucine, corticotropin-releasing factor, angiotensin II, leucine-enkephalin, and methionine-enkephalin-Arg-Gly-Leu.

Immunological Detection of NERPs—Rat hypothalamus was extracted and condensed with a Sep-Pak C18 cartridge as described previously (17). An aliquot of cartridge eluate was examined by RIA to quantify each NERP. The remaining portion was separated by RP-HPLC and assessed by RIA to identify individual immunoreactive (ir-) NERPs. To determine major endogenous forms of rat NERPs, Sephadex G-50 gel-filtrated fractions of rat brain extracts (1.1- and 5.9-g eq for NERP-1 and NERP-2, respectively) were immunoprecipitated with anti-NERP antibodies and then analyzed on a surface-enhanced laser desorption ionization mass spectrometer (Ciphergen, Fremont, CA). Immunoprecipitate from TT cell extract was prepared and mass analyzed as described (14).

Intracerebroventricular Administration—Male Wistar rats (aged 9–10 weeks, from Charles River Laboratories, Shiga, Japan) were maintained in individual cages under controlled temperature (21–23 °C) and light (light on 08:00–20:00) conditions with *ad libitum* access to food and water. Cannulation and intracerebroventricular (icv) administration were performed as described (18). Test materials for icv administration were dissolved in 10 μl of artificial cerebrospinal fluid (aCSF) containing 124 mM NaCl, 5 mM KCl, 1.3 mM $MgSO_4$, 1.24 mM KH_2PO_4, 2 mM $CaCl_2$, 25.9 mM $NaHCO_3$, and 10 mM glucose, pH 7.3. All animal experiments were repeated three to five times and performed in accordance with the guidelines for animal care from the Japanese Physiological Society.

Immunohistochemistry—Brains were removed from colchicine (200 μg)-treated rats following perfusion with either 2% paraformaldehyde (PFA) or 4% PFA containing 0.1% glutaraldehyde, respectively, for immunofluorescence microscopy or electron microscopy. Immunofluorescence staining and immunogold electron microscopy were performed as described previously (19, 20). For light microscopy, peripheral tissues from rats perfused with 2% PFA were stained with antibodies against NERP-1 (1:2,500), rat NERP-2 (1:5,000), oxytocin (1:15,000; Chemicon, Temecula, CA), and vasopressin (1:80,000; Peninsula Laboratories, Torrance, CA). Samples were visualized as described (21). Control studies were done with normal rabbit serum or NERP antisera that had been pretreated with 10 μg of synthetic NERPs.

In Situ Hybridization—VGF and vasopressin mRNA levels in the supraoptic nucleus (SON) and paraventricular nucleus (PVN) from rats deprived of water for 48 h were examined by *in situ* hybridization with ^{33}P 3′ end-labeled deoxyoligonucleotide probes specific for VGF (complementary to bases 1741–1785

[4] The abbreviations used are: RP-HPLC, reversed phase-high performance liquid chromatography; AII, angiotensin II; ir, immunoreactive; MS, mass spectrometry; MS/MS, tandem mass spectrometry; NERP, neuroendocrine regulatory peptide; PFA, paraformaldehyde; PVN, paraventricular nucleus; RIA, radioimmunoassay; SON, supraoptic nucleus; TOF, time-of-flight; RP-HPLC, reversed phase-high performance liquid chromatography; aCSF, artificial cerebrospinal fluid.

and 1825–1870 of rat VGF nucleotides; GenBank™ accession number M74223) and vasopressin (complementary to bases 1843–1868 of rat vasopressin nucleotides) as described (18). Autoradiographic images were analyzed on an MCID imaging analyzer (18). VGF mRNA intensity is expressed relative to that of control rats drinking water *ad libitum* ($n = 5$ per group).

Vasopressin Secretion and Measurements—Rats ($n = 8–14$ per group) received an icv injection of test peptide 5 min before icv injection of either hypertonic NaCl (8.5 μmol of NaCl/10 μl of aCSF) or AII (0.1 nmol/10 μl of aCSF). Plasma vasopressin was measured using an RIA kit (Mitsubishi Chemical, Tokyo, Japan) in blood samples taken 10 min after the hypertonic saline or AII injection. Static incubation of PVN and SON explants punched out from the hypothalamus was performed as reported previously with minor modifications (22). They were sequentially stimulated (each at a final concentration of 10^{-6} M for 5 min) as indicated in Fig. 5. Stimulation periods were separated by 5-min recovery periods. At the end of each experiment, KCl was added at a final concentration of 6×10^{-2} M to confirm depolarization-induced secretion. Perifusion assays were replicated 5–8 times.

Effects of NERPs on Plasma Vasopressin in Rats—Rats ($n = 8$ per group) deprived of water for 48 h were decapitated 10 min after icv administration of NERP-1 or NERP-1-Gly (1nmol/rat) to measure plasma vasopressin. Prior to immunoneutralization studies of NERPs, water (5 ml/100 g body weight) was loaded to rats ($n = 8$ per group) by oral injection through a stomach tube. Fifteen minutes after water loading, rats received an icv injection of anti-NERP-1-IgG (0.1 μg), anti-NERP-2-IgG (0.1 μg), or control IgG (0.1 μg). Rats were decapitated 45 min after immunoneutralization, and plasma vasopressin was measured.

Statistical Analysis—All data are expressed as means ± S.E. Groups of data were compared with analysis of variance and the post-hoc Fisher's test. $p < 0.05$ were considered to be statistically significant.

RESULTS

Peptidomic Identification of NERPs from Culture Supernatant of TT Cells—We analyzed peptides secreted from human medullary thyroid carcinoma TT cells, because this cell line is known to actively secrete the C-terminally amidated peptide hormones calcitonin gene-related peptide α and calcitonin (13). The supernatant of the cell line cultured in a serum-free medium for 6 h was concentrated and subjected to gel filtration chromatography to obtain a peptide-rich fraction, whose cysteine residues were then converted to carboxyamidomethyl cysteine using dithiothreitol and iodoacetamide. This peptide fraction was separated by conventional RP-HPLC to 50 fractions (Fig. 1*A*), each of which was analyzed with tandem mass spectrometric techniques for identification. We identified 19 C-terminally amidated peptides (Fig. 1*B*), of which 15 peptides were the entire or partial sequences corresponding to calcitonin gene-related peptide α and calcitonin. The identification of a series of 13 calcitonin gene-related peptide α-derived (CRGPα) peptides with sequential N-terminal deletions is consistent with the fact that this cell line produces this peptide α at higher levels than calcitonin (13). Of note, we discovered two novel amidated peptides with monoisotopic masses of 2677.4 and 4062.2, both of which were derived from distinct regions of the neurosecretory protein VGF; one is from human VGF-(281–306), and the is other from VGF-(310–347) (NCBI accession number gi|17136078) (Fig. 1, *C* and *D*). Shorter fragments of both peptides were also identified (Fig. 1*B*). Based on their localization and physiological role described below, we designated these peptides as neuroendocrine regulatory peptide (NERP)-1 and NERP-2.

Antisera against NERP-1 and NERP-2—The rat VGF sequences registered in the NCBI data base, as represented by gi|13591864 and gi|1352860, suggest that the rat precursor comprised of 617 amino acids generates amidated peptides as well. To characterize rat endogenous peptides, we prepared antibodies specific to the C-terminal region of each peptide; an octapeptide common to human and rat NERP-1 (QGLAQVEA-NH_2) and decapeptides of rat NERP-2 (QGGARQRDLG-NH_2) and human NERP-2 (QGGARQRGLG-NH_2) were used for immunization. We confirmed that each antiserum strictly recognizes the C-terminal amide structure but does not show more than 0.1% cross-reactivity with its C-terminally Gly-extended peptide or another NERP. Furthermore, the antisera did not recognize rat C-terminal VGF-(588–617) peptide or human C-terminal VGF-(586–615) peptide even at 10 μM, indicating that they do not detect the intact VGF precursor.

Characterization and Identification of NERP-1 and NERP-2—In the Sephadex G-50 gel filtration of rat brain extracts, ir-NERP-1 and ir-NERP-2 were observed as distinctive peaks in the region of relative molecular mass <6 kDa (data not shown). These NERP-1- and NERP-2-immunoreactive fractions were further characterized by mass analysis of immunoprecipitates using these antibodies (Fig. 2, *A* and *B*). Based on the observed mass of the immunoprecipitates, we concluded that rat NERP peptides are derived from the VGF precursor (gi|13591864, Gly at residue 342), with the major endogenous forms of rat NERP-1 and NERP-2 being 25 and 38 amino acids long, respectively (Fig. 1*E*). The rat hypothalamus ir-NERPs behaved identically to synthetic rat NERP-1 or NERP-2 on RP-HPLC (Fig. 2*C*). Immunoprecipitation experiments with TT cell extract also showed the dominant peaks that correspond to human NERP-1 (2677 Da) and NERP-2 (4062 Da). These findings suggest that the processing and amidation of NERPs occur intracellularly before secretion, as is known with amidated bioactive peptides secreted by endocrine cells (7).

NERPs Suppress Vasopressin Release—ir-NERPs were highly abundant in the rat hypothalamus (NERP-1, 14.40 ± 1.05 pmol/g wet weight; NERP-2, 11.33 ± 0.80 pmol/g wet weight, $n = 5$). Cell bodies with strong immunostaining of NERPs were observed in the SON (Fig. 3, *A–D*) and PVN (Fig. 3, *E–J*), the nuclei that produce vasopressin and oxytocin (23, 24). Immunofluorescence microscopy showed that NERPs frequently colocalized with vasopressin, which controls body fluid homeostasis, but rarely with oxytocin (Fig. 3, *A–D*). Within the PVN, immunostaining of NERPs was detected in both magnocellular and parvocellular divisions, whereas that of arginine vasopressin was mainly observed in the magnocellular division. Thus, arginine vasopressin-pos-

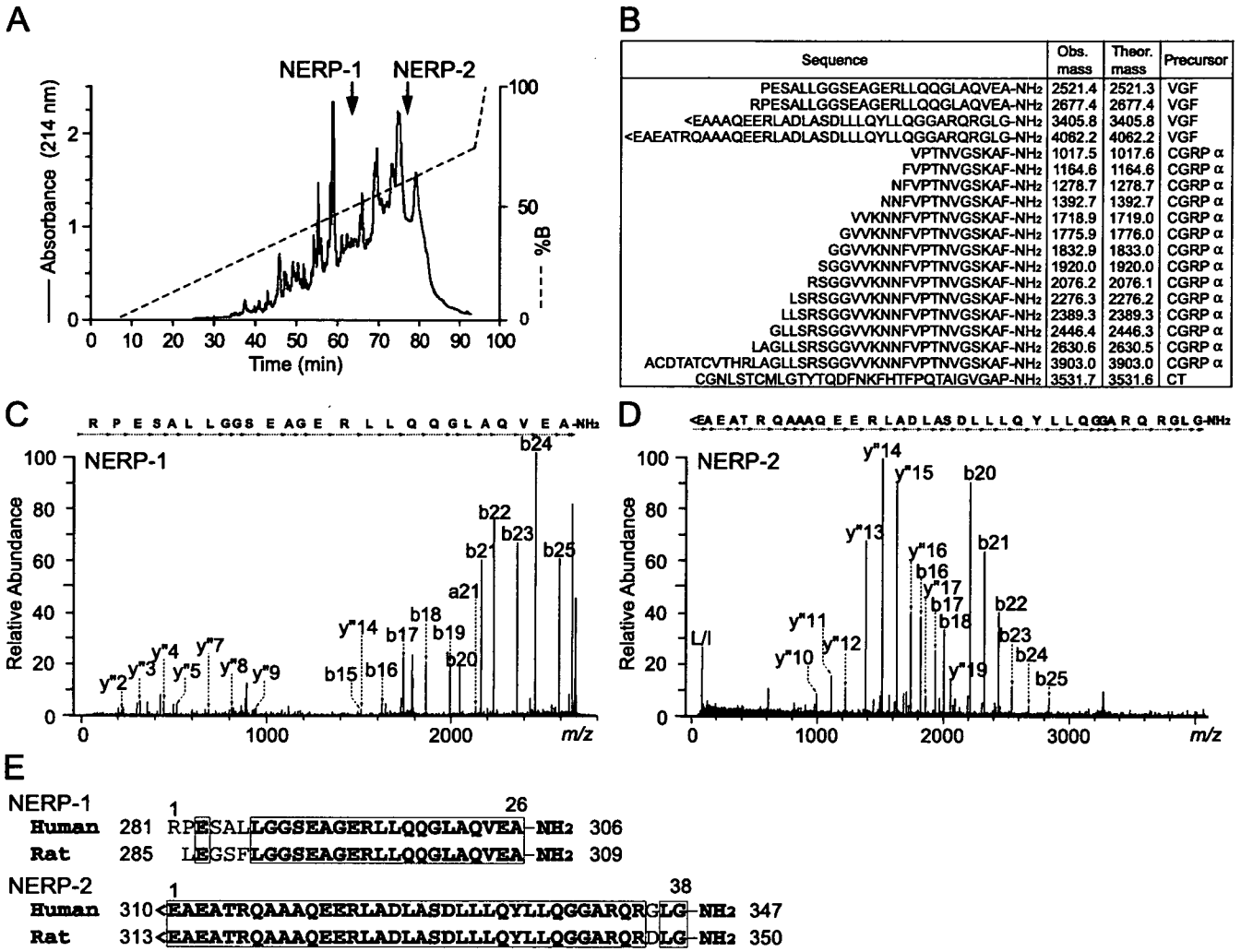

Sequence	Obs. mass	Theor. mass	Precursor
PESALLGGSEAGERLLQQGLAQVEA-NH2	2521.4	2521.3	VGF
RPESALLGGSEAGERLLQQGLAQVEA-NH2	2677.4	2677.4	VGF
<EAAAQEERLADLASDLLLQYLLQGGARQRGLG-NH2	3405.8	3405.8	VGF
<EAEATRQAAAQEERLADLASDLLLQYLLQGGARQRGLG-NH2	4062.2	4062.2	VGF
VPTNVGSKAF-NH2	1017.5	1017.6	CGRP α
FVPTNVGSKAF-NH2	1164.6	1164.6	CGRP α
NFVPTNVGSKAF-NH2	1278.7	1278.7	CGRP α
NNFVPTNVGSKAF-NH2	1392.7	1392.7	CGRP α
VVKNNFVPTNVGSKAF-NH2	1718.9	1719.0	CGRP α
GVVKNNFVPTNVGSKAF-NH2	1775.9	1776.0	CGRP α
GGVVKNNFVPTNVGSKAF-NH2	1832.9	1833.0	CGRP α
SGGVVKNNFVPTNVGSKAF-NH2	1920.0	1920.0	CGRP α
RSGGVVKNNFVPTNVGSKAF-NH2	2076.2	2076.1	CGRP α
LSRSGGVVKNNFVPTNVGSKAF-NH2	2276.3	2276.2	CGRP α
LLSRSGGVVKNNFVPTNVGSKAF-NH2	2389.3	2389.3	CGRP α
GLLSRSGGVVKNNFVPTNVGSKAF-NH2	2446.4	2446.3	CGRP α
LAGLLSRSGGVVKNNFVPTNVGSKAF-NH2	2630.6	2630.5	CGRP α
ACDTATCVTHRLAGLLSRSGGVVKNNFVPTNVGSKAF-NH2	3903.0	3903.0	CGRP α
CGNLSTCMLGTYTQDFNKFHTFPQTAIGVGAP-NH2	3531.7	3531.6	CT

FIGURE 1. **Peptidomic identification of NERPs.** *A*, RP-HPLC of the secretory peptides obtained from culture supernatant of TT cells. NERP-1 (2677.4 Da) and NERP-2 (4062.2 Da) were eluted at the positions indicated by *arrows*. *B*, summary of C-terminally amidated peptides. <*E*, pyroglutamic acid; *Obs*, observed; *Theor*, theoretical. *C* and *D*, identification of NERP-1 (*C*) and NERP-2 (*D*) by nano-electrospray ionization MS/MS. MS/MS spectra were obtained from the precursor ions at *m/z* 893.5 ($[M + 3H]^{3+}$ ion) (*C*) and *m/z* 1016.5 ($[M + 4H]^{4+}$ ion) (*D*). The resultant spectra, deconvoluted with MaxEnt3TM (Micromass), were interpreted by SeqMS (15). The *y"n* and bm ions, where *n* and *m* denote arbitrary positions counted from the C and N termini, indicate C- and N-terminal ions, respectively, which were produced by cleavage of peptide bonds during MS/MS. *L/I* in the spectrum (*D*) denotes the immonium ion of Leu or Ile, which have the same mass. *E*, sequence alignment of human and rat NERPs. Residue numbering is based on the human (gi|17136078) and rat (gi|13591864) VGF precursor.

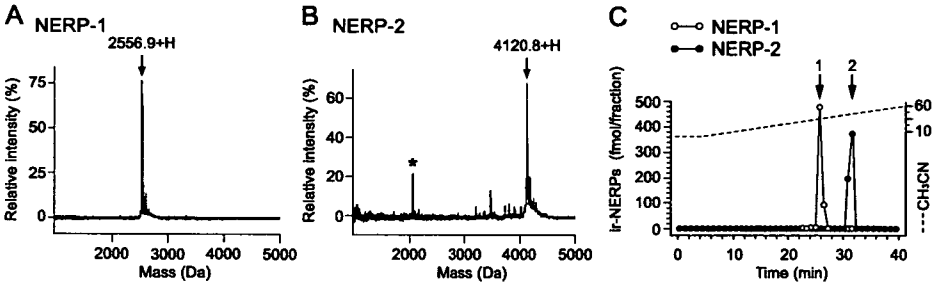

FIGURE 2. **Major endogenous forms of rat NERPs determined by surface-enhanced laser desorption ionization mass spectrometry and RP-HPLC.** Peptides immunoprecipitated with an antibody against NERP-1 (*A*) or NERP-2 (*B*) from rat brain extracts were analyzed. The values correspond to the molecular masses of 25-amino acid-long NERP-1 (*A*, VGF-(285–309)) and 38-amino acid-long NERP-2 (*B*, VGF-(313–350)) of rat VGF (gi|13591864). An *asterisk* denotes a doubly charged ion. *C*, characterization of ir-NERPs from rat hypothalamus by RP-HPLC coupled with RIAs. *Arrows 1* and *2* indicate the elution positions of synthetic rat NERP-1 and NERP-2.

itive cells are concluded to contain NERPs at high frequency. Immunogold electron microscopy revealed the colocalization of NERPs with vasopressin in storage granules (Fig. 3, *A* and *C*, *insets*). Based on these results, we supposed that we could elucidate a biological function of NERPs in the context of vasopressin physiology.

VGF mRNA levels in both the PVN and SON were up-regulated upon water deprivation in rats (Fig. 4, *A* and *B*), accompanied by the up-regulation of vasopressin mRNA levels (PVN, 153.0 ± 13.6%; SON, 161.9 ± 12.4%; % of controls, $p < 0.01$). These *in vivo* and immunocytochemical observations suggest that NERPs are involved in the central control of body fluid balance. Consistent with previous reports (25, 26), icv injection of hypertonic NaCl or AII increased plasma vasopressin levels in rats (Fig. 4*C*, *2nd* and

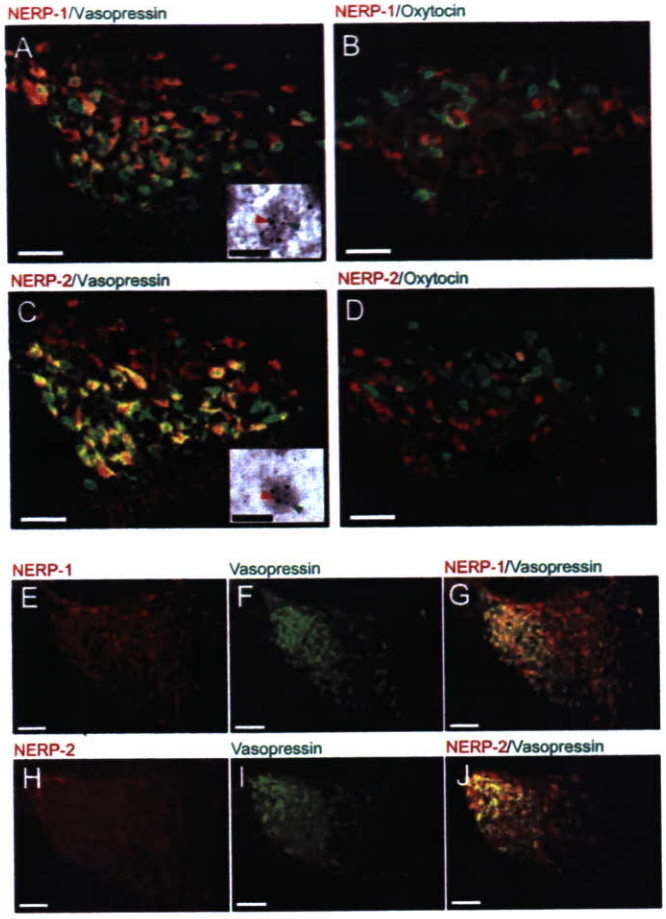

FIGURE 3. **NERPs colocalize with vasopressin in the PVN and SON of rats.** *A–D*, NERPs-specific immunohistochemistry of the SON. NERP-1 and NERP-2 (both in *red*) frequently colocalize with vasopressin (*green*) but rarely with oxytocin (*green*). *Scale bars*, 50 μm. *Inset*, immunoelectron micrographs indicating the colocalization of NERPs (10-nm gold particles, *red arrowhead*) with vasopressin (5-nm gold particles, *green arrowhead*) in an SON neuron. *Scale bars*, 1 μm. *E–J*, immunofluorescence staining of NERPs in the PVN. NERP-1 and NERP-2 (both in *red*) colocalize with vasopressin (*green*), especially in the magnocellular division. *Scale bars*, 100 μm.

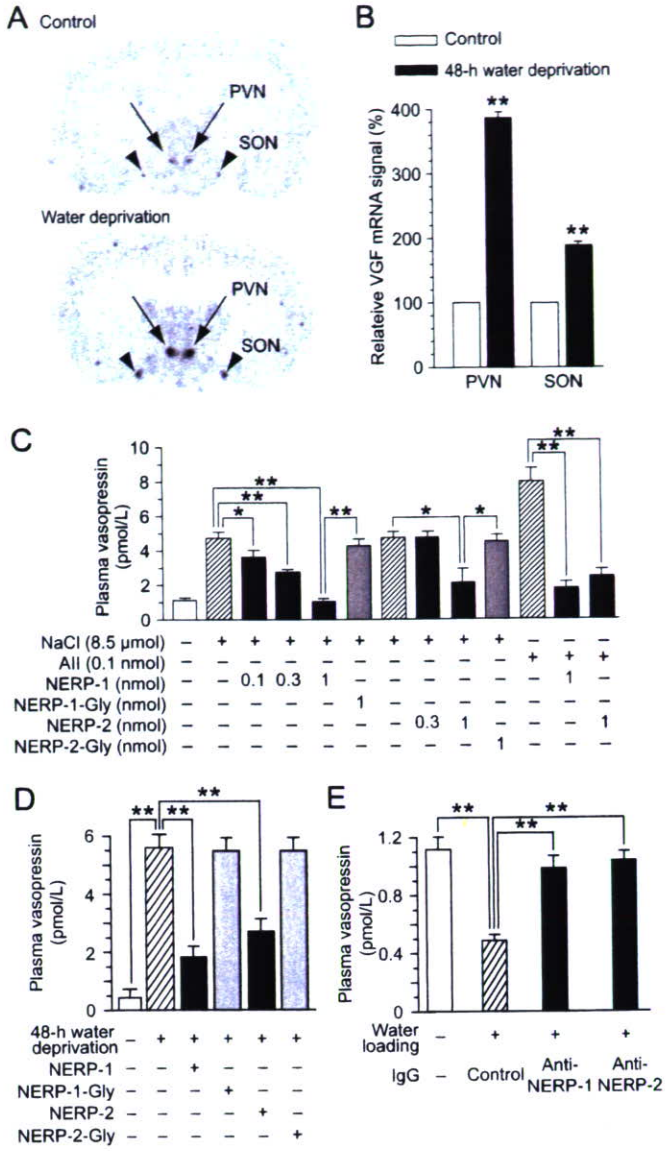

FIGURE 4. **NERPs suppress vasopressin secretion *in vivo* in rats.** *A*, increased VGF gene expression in the PVN and SON following 48 h of water deprivation. *B*, quantitative densitometric analysis of *A*. *C*, effect of icv-administered NERPs on rat plasma vasopressin levels in response to icv stimulation with hypertonic NaCl or AII. *D*, intracerebroventricular administration of NERPs, but neither NERP-1-Gly nor NERP-2-Gly, to rats suppressed plasma vasopressin elevation induced by water deprivation. *E*, intracerebroventricular administration of anti-NERP-1 IgG or anti-NERP-2 IgG reversed plasma vasopressin suppression induced by water loading. *, $p < 0.05$; **, $p < 0.01$.

11th lanes). This stimulation was dose-dependently suppressed by icv injection of NERP-1 before injection of the vasopressin secretagogues (Fig. 4*C*). Similar effects were observed with NERP-2, but its potency was weaker than that of NERP-1 because 0.3 nmol of NERP-2 was not effective. Neither nonamidated NERP-1 (NERP-1-Gly) nor nonamidated NERP-2 (NERP-2-Gly) suppressed vasopressin secretion (Fig. 4*C*). The increase in plasma vasopressin levels caused by water deprivation was also suppressed by icv-administered NERP-1 or NERP-2 (Fig. 4*D*). Furthermore, icv administration of anti-NERP-1 IgG or anti-NERP-2 IgG significantly reversed plasma vasopressin suppression induced by acute water loading (Fig. 4*E*), suggesting that NERPs function as endogenous peptides to regulate vasopressin secretion. Next, we examined the *in vitro* effect of NERPs on vasopressin secretion using hypothalamic explants. NERP-1 suppressed basal and AII-induced vasopressin secretion from the PVN and SON (Fig. 5). NERP-2 was likewise effective, but NERP-1-Gly or NERP-2-Gly was not (Fig. 5).

DISCUSSION

In this study, to expedite the identification of potentially bioactive peptides, we analyzed peptides present in the supernatant of cultured cells, rather than analyzing peptides extracted from tissues. In addition, the benefit of our approach is that we examined an endocrine cell line that secretes C-terminally amidated peptide hormones such as calcitonin or calcitonin gene-related peptide at a high rate. Because C-terminal amidation is a post-translational modification most often shared by bioactive peptides (7), we thought that potentially bioactive peptides could be identified easier using this chemical feature. This tag has been used to discover a series of bioactive peptides such as

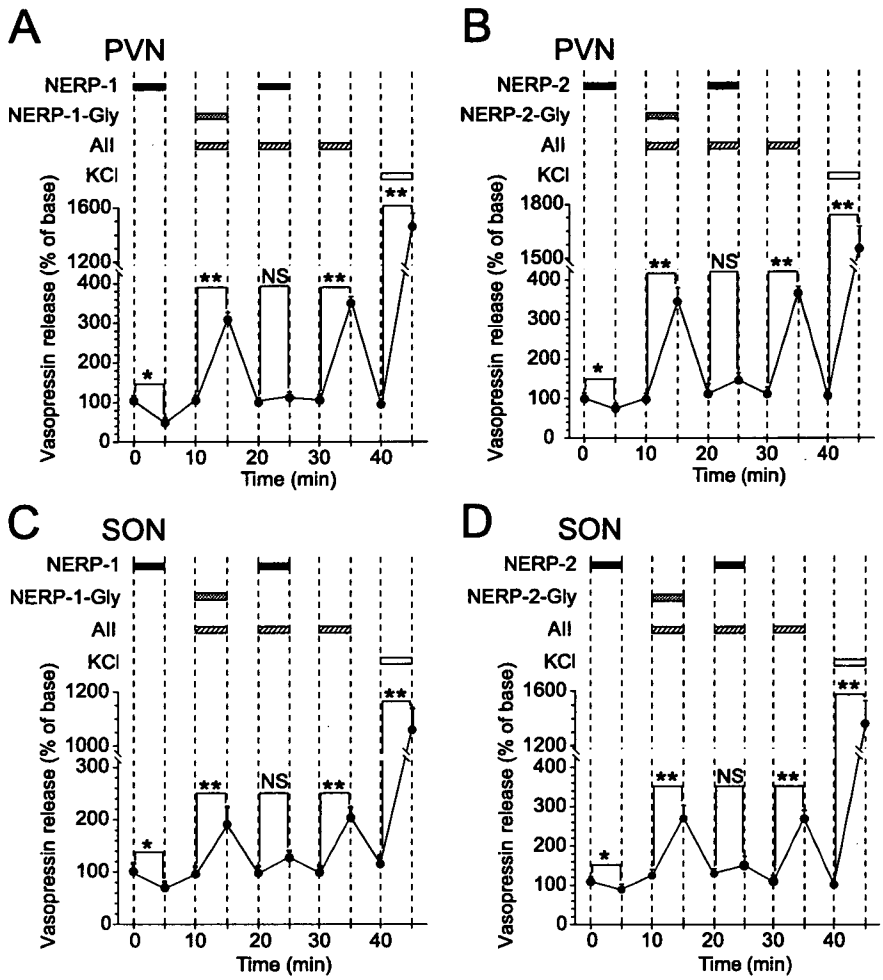

FIGURE 5. **NERPs suppress vasopressin secretion from PVN (*A* and *B*) and SON (*C* and *D*) explants.** *Black, gray, shaded,* and *white bars* indicate the NERPs, NERPs-Gly, AII, and KCl administration periods, respectively. *, $p < 0.05$; **, $p < 0.01$; NS, not significant.

galanin or neuropeptide Y (27). Using this "peptide first" approach, it remains difficult to infer biological activity just from the sequence of a peptide even if it is C-terminally amidated. Fortuitously, localization of NERPs in specific hypothalamic nuclei allowed us to speculate on their possible biological roles in relation to known peptide hormone, vasopressin, and to analyze them with *in vitro* and *in vivo* experiments described here.

VGF, originally identified in rat pheochromocytoma PC12 cells as a nerve growth factor-responsive gene, encodes a 617-amino acid protein in rodents (8). Immunohistochemical studies in PC12 cells revealed that the protein is stored in dense core granules and secreted through the regulated pathway (28, 29). Because VGF harbors several paired basic amino acid residues targeted by prohormone convertases, it has long been considered a precursor for several bioactive peptides (9). Using antibodies raised against the C terminus of the intact VGF protein, some VGF-derived peptides have been reported and shown to possess biological activity; C-terminal peptides TLQP-62 and AQEE-30 enhance synaptic activity in a whole-cell patch clamp recording on rat hippocampal cells (30), and AQEE-30 and LQEQ-19 enhance penile erection (31). More recently, the study has extended to the identification of TLQP-21 that increases energy expenditure by stimulating autonomic activation of adrenal medulla and adipose tissues (10).

In contrast to these conventional approaches, several peptidomics studies have reported the identification of VGF-derived peptides in brain tissues or cerebrospinal fluid (11, 12). Some VGF peptides are reported to be a marker for Alzheimer disease (32, 33). Except for the aforementioned VGF peptides, however, no VGF-related peptides have been demonstrated to be bioactive. Current peptidomic studies use tandem mass spectrometric techniques for peptide identification, in which C-terminal amidation is considered as a possible modification that target peptides could undergo. Because mass spectrometry schemes tend to detect abundant peptides or easily ionized peptides, it would make sense that no C-terminally amidated peptides from VGF have been reported to date.

It should also be mentioned that NERP-2 might have escaped *in silico* prediction of bioactive peptides that principally takes into account only paired basic amino acid residues for processing sites; human and rat NERP-2 are cleaved at the amino acid residues ^{345}GLG↓GRG^{350} and ^{348}DLG↓GRG^{353}, respectively. The identification of these processing sites also demonstrates a methodological advantage of a peptidomic approach, and *in silico* prediction in turn may also be reinforced by accumulating data about endogenous peptides that peptidomics is going to provide.

Vasopressin synthesized in the PVN and SON magnocellular neurosecretory cells is packed in the secretory granules. Axons from these cells terminate in the posterior pituitary from which vasopressin is secreted into the systemic circulation to control renal excretion of water. NERPs were frequently colocalized with vasopressin in the secretory granules of the PVN and SON. VGF mRNA levels increased along with vasopressin mRNA in response to water deprivation, suggesting that NERPs participate in the hypothalamic control of plasma osmolarity balance. Both NERP-1 and NERP-2 suppressed vasopressin release stimulated by icv administration of hypertonic saline or AII *in vivo*. In *in vitro* experiments, NERPs also abolished AII-induced vasopressin release from the PVN and SON. All these actions were observed with C-terminally amidated forms only. Both anti-NERPs IgGs canceled plasma vasopressin reduction in

response to water loading, indicating that NERPs could be potent endogenous suppressors of vasopressin release.

Vasopressin release is regulated by the electrical activity of vasopressin neurons, which are modulated by various neurotransmitters and neuromodulators (25, 26). The major neural signals to vasopressin neurons are excitatory and inhibitory postsynaptic currents generated by presynaptic release of glutamate and γ-aminobutyric acid, respectively. AII and NaCl potentiate excitatory postsynaptic currents in vasopressin neurons, thereby stimulating vasopressin secretion (25). Although cell-surface receptors or target proteins of NERPs have not been identified yet, the actions of NERP to suppress AII- and NaCl-induced vasopressin release from the hypothalamus may suggest that they presynaptically inhibit the glutamatergic inputs or enhance GABAergic inputs to vasopressin neurons. Further investigation using whole-cell patch clamp recordings of PVN or SON slice preparations to examine the effect of NERPs on synaptic inputs to vasopressin neurons should elucidate the mechanisms by which NERPs modulate vasopressin release.

In conclusion, NERPs are novel bioactive peptides involved in body fluid homeostasis; they appear to modulate the actions and secretions of other neuropeptides. This study exemplifies the ability of focused peptidomics to facilitate the discovery of mammalian bioactive peptides. Further studies of NERPs and their receptors will pave the way for elucidating unknown extracellular signaling mechanisms as well as understanding the physiological roles of NERPs in body fluid homeostasis.

Acknowledgments—We thank J. Isoyama-Tanaka, T. Tsuruta, T. Matsuo, and R. Matsuura for expert technical assistance.

REFERENCES

1. Zhou, A., Webb, G., Zhu, X., and Steiner, D. F. (1999) *J. Biol. Chem.* **274,** 20745–20748
2. Schrader, M., and Schulz-Knappe, P. (2001) *Trends Biotechnol.* **19,** S55–S60
3. Clynen, E., Baggerman, G., Veelaert, D., Cerstiaens, A., van der Horst, D., Harthoorn, L., Derua, R., Waelkens, E., De Loof, A., and Schoofs, L. (2001) *Eur. J. Biochem.* **268,** 1929–1939
4. Minamino, N., Tanaka, J., Kuwahara, H., Kihara, T., Satomi, Y., Matsubae, M., and Takao, T. (2003) *J. Chromatogr. B.* **792,** 33–48
5. Svensson, M., Skold, K., Svenningsson, P., and Andren, P. E. (2003) *J. Proteome Res.* **2,** 213–219
6. Che, F. Y., Vathy, I., and Fricker, L. D. (2006) *J. Mol. Neurosci.* **28,** 265–275
7. Eipper, B. A., Stoffers, D. A., and Mains, R. E. (1992) *Annu. Rev. Neurosci.* **15,** 57–85
8. Levi, A., Eldridge, J. D., and Paterson, B. M. (1985) *Science* **229,** 393–395
9. Levi, A., Ferri, G. L., Watson, E., Possenti, R., and Salton, S. R. (2004) *Cell. Mol. Neurobiol.* **24,** 517–533
10. Bartolomucci, A., La Corte, G., Possenti, R., Locatelli, V., Rigamonti, A. E., Torsello, A., Bresciani, E., Bulgarelli, I., Rizzi, R., Pavone, F., D'Amato, F. R., Severini, C., Mignogna, G., Giorgi, A., Schinina, M. E., Elia, G., Brancia, C., Ferri, G. L., Conti, R., Ciani, B., Pascucci, T., Dell'Omo, G., Muller, E. E., Levi, A., and Moles, A. (2006) *Proc. Natl. Acad. Sci. U. S. A.* **103,** 14584–14589
11. Yuan, X., and Desiderio, D. M. (2005) *J. Mass. Spectrom.* **40,** 176–181
12. Lim, J., Berezniuk, I., Che, F. Y., Parikh, R., Biswas, R., Pan, H., and Fricker, L. D. (2006) *J. Neurochem.* **4,** 1169–1181
13. Gkonos, P. J., Born, W., Jones, B. N., Petermann, J. B., Keutmann, H. T., Birnbaum, R. S., Fischer, J. A., and Roos, B. A. (1986) *J. Biol. Chem.* **261,** 14386–14391
14. Sasaki, K., Sato, K., Akiyama, Y., Yanagihara, K., Oka, M., and Yamaguchi, K. (2002) *Cancer Res.* **62,** 4894–4898
15. Fernandez-de-Cossio, J., Gonzalez, J., Satomi, Y., Shima, T., Okumura, N., Besada, V., Betancourt, L., Padron, G., Shimonishi, Y., and Takao, T. (2000) *Electrophoresis* **21,** 1694–1699
16. Katafuchi, T., Kikumoto, K., Hamano, K., Kangawa, K., Matsuo, H., and Minamino, N. (2003) *J. Biol. Chem.* **278,** 12046–12054
17. Mondal, M. S., Nakazato, M., Date, Y., Murakami, N., Yanagisawa, M., and Matsukura, S. (1999) *Biochem. Biophys. Res. Commun.* **256,** 495–499
18. Nakazato, M., Murakami, N., Date, Y., Kojima, M., Matsuo, H., Kangawa, K., and Matsukura, S. (2001) *Nature* **409,** 194–198
19. Toshinai, K., Date, Y., Murakami, N., Shimada, M., Mondal, M. S., Shimbara, T., Guan, J. L., Wang, Q. P., Funahashi, H., Sakurai, T., Shioda, S., Matsukura, S., Kangawa, K., and Nakazato, M. (2003) *Endocrinology* **144,** 1506–1512
20. Gies, U., and Theodosis, D. T. (1994) *J. Neurosci.* **14,** 2861–2869
21. Date, Y., Ueta, Y., Yamashita, H., Yamaguchi, H., Matsukura, S., Kangawa, K., Sakurai, T., Yanagisawa, M., and Nakazato, M. (1999) *Proc. Natl. Acad. Sci. U. S. A.* **96,** 748–753
22. Beak, S. A., Heath, M. M., Small, C. J., Morgan, D. G., Ghatei, M. A., Taylor, A. D., Buckingham, J. C., Bloom, S. R., and Smith, D. M. (1998) *J. Clin. Investig.* **101,** 1334–1341
23. Bondy, C. A., Whitnall, M. H., Brady, L. S., and Gainer, H. (1989) *Cell. Mol. Neurobiol.* **4,** 427–446
24. Ludwig, M., Sabatier, N., Dayanithi, G., Russell, J. A., and Leng, G. (2002) *Prog. Brain Res.* **139,** 247–256
25. Yamashita, H., Ueta, Y., and Dyball, E. R. (2002) in *Hormones, Brain, and Behavior* (Pfaff, D. W., Arnold, A. P., Etgen, A. M., Fahrbach, S. E., and Rubin, R. T., eds) Vol. 160, pp. 1–49, Academic Press, New York
26. Wells, T., and Forsling, M. L. (1992) *J. Physiol. Pharmacol.* **43,** 59–64
27. Tatemoto, K., and Mutt, V. (1980) *Nature* **285,** 417–418
28. Possenti, R., Eldridge, J. D., Paterson, B. M., Grasso, A., and Levi, A. (1989) *EMBO J.* **8,** 2217–2223
29. Benson, D. L., and Salton, S. R. (1996) *Brain Res. Dev. Brain Res.* **96,** 219–228
30. Alder, J., Thakker-Varia, S., Bangasser, D. A., Kuroiwa, M., Plummer, M. R., Shors, T. J., and Black, I. B. (2003) *J. Neurosci.* **23,** 10800–10808
31. Succu, S., Cocco, C., Mascia, M. S., Melis, T., Melis, M. R., Possenti, R., Levi, A., Ferri, G. L., and Argiolas, A. (2004) *Eur. J. Neurosci.* **20,** 3035–3040
32. Carrette, O., Demalte, I., Scherl, A., Yalkinoglu, O., Corthals, G., Burkhard, P., Hochstrasser, D. F., and Sanchez, J. C. (2003) *Proteomics* **3,** 1486–1494
33. Huang, J. T., Leweke, F. M., Oxley, D., Wang, L., Harris, N., Koethe, D., Gerth, C. W., Nolden, B. M., Gross, S., Schreiber, D., Reed, B., and Bahn, S. (2006) *PloS. Med.* **3,** e428

GLIA 55:604–616 (2007)

Involvement of $P2X_4$ and $P2Y_{12}$ Receptors in ATP-Induced Microglial Chemotaxis

KEIKO OHSAWA,[1] YASUHIRO IRINO,[1] YASUKO NAKAMURA,[1] CHIHIRO AKAZAWA,[1] KAZUHIDE INOUE,[2] AND SHINICHI KOHSAKA[1]*

[1]*Department of Neurochemistry, National Institute of Neuroscience, Kodaira, Tokyo 187-8502, Japan*

[2]*Department of Pharmacology, Graduate School of Pharmaceutical Sciences, Kyushu University, Higashi, Fukuoka 812-8582, Japan*

KEY WORDS
microglia; ATP; chemotaxis; P2Y12; P2X4

ABSTRACT
We previously reported that extracellular ATP induces membrane ruffling and chemotaxis of microglia and suggested that their induction is mediated by the Gi/o-protein coupled $P2Y_{12}$ receptor ($P2Y_{12}R$). Here we report discovering that the $P2X_4$ receptor ($P2X_4R$) is also involved in ATP-induced microglial chemotaxis. To understand the intracellular signaling pathway downstream of $P2Y_{12}R$ that underlies microglial chemotaxis, we examined the effect of two phosphatidylinositol 3′-kinase (PI3K) inhibitors, wortmannin, and LY294002, on chemotaxis in a Dunn chemotaxis chamber. The PI3K inhibitors significantly suppressed chemotaxis without affecting ATP-induced membrane ruffling. ATP stimulation increased Akt phosphorylation in the microglia, and the increase was reduced by the PI3K inhibitors and a $P2Y_{12}R$ antagonist. These results indicate that $P2Y_{12}R$-mediated activation of the PI3K pathway is required for microglial chemotaxis in response to ATP. We also found that the Akt phosphorylation was reduced when extracellular calcium was chelated, suggesting that ionotropic P2X receptors are involved in microglial chemotaxis by affecting the PI3K pathway. We therefore tested the effect of various $P2X_4R$ antagonists on the chemotaxis, and the results showed that pharmacological blockade of $P2X_4R$ significantly inhibited it. Knockdown of the $P2X_4$ receptor in microglia by RNA interference through the lentivirus vector system also suppressed the microglial chemotaxis. These results indicate that $P2X_4R$ as well as $P2Y_{12}R$ is involved in ATP-induced microglial chemotaxis.

INTRODUCTION

Microglia are the immune effector cells that participate in tissue repair, amplification of inflammatory responses, and neuronal degeneration in the central nervous system (CNS) (Kreutzberg, 1996; Streit, 2002). They are present in the form of ramified cells under normal conditions, but in response to pathological stimuli microglia rapidly transform into a motile ameboid form and migrate toward lesion sites, where they secrete a variety of substances and clear cell debris (Moran and Graeber, 2004; Nakajima and Kohsaka, 2005; Stence et al., 2001). Thus, microglial migration plays a crucial role in the amelioration of a damaged CNS; however, the intracellular signals underlying microglial cell migration are poorly understood.

Extracellular ATP is known to play a role as a neurotransmitter or neuromodulator in the CNS (Illes and Alexandre Ribeiro, 2004), and it regulates various physiological functions of microglia (Inoue, 2002). ATP receptors are classified into two families: the ionotropic P2X receptor (P2XR) family and the GTP-binding (G-) protein coupled P2Y receptor (P2YR) family (Ralevic and Burnstock, 1998), and microglia have been reported to possess functional ATP receptors, including $P2X_4R$, $P2X_7R$, and $P2Y_{12}R$ (Cavaliere et al., 2003; James and Butt, 2002; Sasaki et al., 2003; Tsuda et al., 2003). Davalos et al. (2005) and Nimmerjahn et al. (2005) recently reported that processes of ramified microglia extended toward a confocal laser injury, where ATP is likely to be released by damaged tissue and surrounding astrocytes. These observations suggest that ATP is a primary molecule in the induction of the change in microglial morphology.

We have also previously reported that ATP-induced microglial membrane ruffling and chemotaxis are mediated by Gi/o-protein coupled $P2Y_{12}R$ (Honda et al., 2001; Sasaki et al., 2003); however, the intracellular signaling pathway downstream of $P2Y_{12}R$ following ATP stimulation is not fully understood. Several recent articles have revealed that $P2Y_{12}R$ stimulation results in activation of the phosphatidylinositol 3′-kinase (PI3K) pathway in some cells (Czajkowski et al., 2004; Soulet et al., 2004; Van Kolen and Slegers, 2004). Although PI3K is known to be a crucial enzyme in the regulation of chemotaxis by monocytes and macrophages (Procko and McColl, 2005; Ridley, 2001; Van Haastert and Devreotes, 2004), whether the PI3K pathway participates in ATP-induced microglial chemotaxis remained unclear.

This article contains supplementary material available via the Internet at http://www.interscience.wiley.com/jpages/0894-1491/suppmat

Grant sponsors: Japanese Ministry of Health, Labour, and Welfare; Japanese Ministry of Education, Culture, Sports, Science, and Technology.

*Correspondence to: Shinichi Kohsaka, Department of Neurochemistry, National Institute of Neuroscience, 4-1-1 Ogawahigashi, Kodaira, Tokyo 187-8502, Japan. E-mail: kohsaka@ncnp.go.jp

Received 7 August 2006; Accepted 26 December 2006

DOI 10.1002/glia.20489

Published online 13 February 2007 in Wiley InterScience (www.interscience.wiley.com).

In this study we demonstrated that activation of the PI3K pathway is required for ATP-induced microglial chemotaxis and found that the PI3K/Akt activation was suppressed when extracellular Ca^{2+} was chelated. ATP stimulates P2XRs in microglia and causes an increase in intracellular calcium concentration ($[Ca^{2+}]_i$) by inducing an extracellular Ca^{2+} influx (Inoue et al., 1998; Tsuda et al., 2003). Therefore, to clarify involvement of P2XRs in microglial chemotaxis we also examined the effect of antagonists and RNA interference (RNAi) with P2XRs on microglial chemotaxis, and the results demonstrated that P2X$_4$R is involved in ATP-induced chemotaxis.

MATERIALS AND METHODS

Isolation of Microglia

Microglia were obtained from primary cell cultures of neonatal Wistar rat cerebral cortex as described previously (Nakajima et al., 1992). In brief, mixed glial cultures were maintained for 12–23 days in DMEM (Invitrogen, Carlsbad, CA) with 10% fetal calf serum (FCS) (Irvine Scientific, Santa Ana, CA). Microglia were prepared as floating cells by gentle shaking and allowed to attach to appropriate dishes or glasses.

Membrane Ruffling

Microglia attached to glass coverslips were incubated for 4 h in DMEM without FCS and stimulated with 50 μM ATP (Yamasashyoyu, Chiba, Japan) for 5 min at 37°C. The cells were then fixed with 3.7% formaldehyde for 10 min, permeabilized for 5 min with PBS containing 0.1% Triton X-100, and stained for 1 h with 2 U/mL Texas Red-conjugated phalloidin (Invitrogen) diluted in PBS containing 1%BSA. The cells were mounted in PermaFluor (Thermo Fisher Scientific, Waltham, MA) and examined under a fluorescence microscope AX70 (Olympus, Tokyo, Japan). To quantify membrane ruffles, cells were stained with 1 μg/mL anti-Iba1 polyclonal antibody (Imai et al., 1996) and Alexa Fluor 488-conjugated anti-rabbit IgG (1:1,000, Invitrogen) and then incubated with 2 U/mL Alexa Fluor 647-conjugated phalloidin (Invitrogen). The F-actin content of cells positive for Iba1 was quantified as the integral intensity of Alexa Fluor 647 fluorescence with a laser scanning cytometer (LSC2, CompuCyte, Cambridge, MA). The mean fluorescent intensity of the cells pretreated with each inhibitor was calculated from the data obtained from 1,000 cells. Increases in membrane ruffles are reported as ratios of the mean fluorescent intensity of the ATP-stimulated cells to that of the unstimulated cells. The effect of the inhibitors was assessed by preincubating cells with wortmannin (Sigma, St. Louis, MO) (100 nM) for 20 min, LY294002 (Wako, Osaka Japan) (50 μM) for 20 min, AR-C69931MX (AstraZeneca, UK) (1 μM) for 10 min, 2′,3′-*O*-(2,4,6-trinitrophenyl) adenosine 5-triphosphate (TNP-ATP) (Invitrogen) (100 μM) for 5 min, pyridoxal-phosphate-6-azophenyl-2′,4′-disulfonic acid (PPADS) (Sigma) (300 μM) for 5 min, or Brilliant blue G (BBG) (Nacalai Tesque, Kyoto, Japan) (1 μM) for 5 min, and then stimulating them with ATP.

Chemotaxis Assay

Dunn chemotaxis chambers (Weber Scientific International, Teddington, UK) were used to perform the chemotaxis assays according to the method described previously (Honda et al., 2001; Webb et al., 1996). In brief, microglia attached to square coverslips were incubated for 4 h in DMEM without FCS. Each coverslip was then inverted onto a chamber and the medium in the outer well was replaced with DMEM containing 50 μM ATP. The chamber was placed on the stage of a microscope (ECLIPSE TE300; Nikon, Tokyo Japan), and cell images were collected every 5 min for 1 h with a CCD camera (Hamamatsu Photonics, Hamamatsu, Japan) and imaging software (fishPPC; Hamamatsu Photonics). Time-lapse video images were used to calculate the final position of cells relative to their starting position, and the distance each cell migrated was measured by plotting the positions of the cell nucleus on a computer display with software (Image-Pro Plus; Media Cybernetics, MD). The distance and direction moved are shown as x and y coordinates on scatter diagrams in which the x-axis is parallel to the outer ring and the position of the outer well is above the y-axis.

Akt Activation

Microglia were incubated for 4 h in DMEM without FCS and then stimulated with 50 μM ATP or 100 ng/mL recombinant murine macrophage-colony stimulating factor (M-CSF) (R&D Systems, Minneapolis, MN) for 5 min at 37°C, and lysed with SDS sample buffer. Proteins were separated by 10% SDS-PAGE and transferred onto an Immobilon P membrane (Millipore, MA). The membrane was incubated for 1 h at room temperature with a blocking solution containing 25 mM Tris, pH 7.5, 150 mM NaCl, 0.1%(v/v) Tween 20 (TTBS), and 5% (v/v) nonfat dry milk, and then incubated overnight at 4°C with mouse monoclonal anti-phospho-Akt (Ser473) antibody (diluted 1:1,000, Cell Signaling Technology, Beverly, MA) or rabbit polyclonal Akt antibody (diluted 1:1,000, Cell Signaling Technology). The membrane was incubated for 1 h at room temperature with horseradish peroxidase (HRP)-conjugated donkey anti-mouse IgG (diluted 1:1,000, GE Healthcare, Little Chalfont, UK) or HRP-conjugated donkey anti-rabbit IgG (diluted 1:1,000, GE Healthcare), and phosphorylated Akt and total Akt were detected with an ECL Western blotting detection system (GE Healthcare). The Akt phosphorylation level was quantified by densitometry with NIH image software. Before stimulating the cells in the calcium-depleted experiment, they were incubated for 30 min in a balanced salt solution composed of 20 mM Hepes, pH7.4, 150 mM NaCl, 5 mM KCl, 1.2 mM $MgCl_2$, and 10 mM glucose in the presence of 1.2 mM Ca^{2+} (BSS) or 1 mM ethy-

lene glycol-*bis*(2-aminoethyl)-*N,N,N′,N′*-tetraacetic acid (EGTA) (Ca^{2+}-free BSS).

Construction of Lentivirus Vectors Expressing Interfering Short Hairpin RNA (shRNAi) and Microglial Transduction

Lentivirus containing shRNAi was prepared by the method previously described (Yogosawa et al., 2005). The self-inactivating (SIN) vector construct pCS-RfA-CG, which contains the EGFP gene under the control of the CMV promoter and sites for site-specific recombination with a Gateway vector (attR1,2), was used for simultaneous expression of EGFP and shRNA. Plasmid containing $P2X_4R$ shRNAi under the control of human U6 promoter was provided by Dr. K. Inoue (Kyushu Univ. Fukuoka, Japan). The gene of the $P2X_4R$ shRNAi-expressing cassette inserted into pENTR™1A was transferred into the pCS-RfA-CG by a recombination reaction using Gateway LR Clonase (Invitrogen). The sequence of shRNA targeted for firefly luciferase was used as a control (Nishitsuji et al., 2004). The sequence was inserted into the piGENE™ hU6 *Bsp*MI vector (iGENE Therapeutics, Tsukuba, Japan), and the gene of the luciferase shRNAi-expressing cassette was ligated into the pCS-RfA-CG. The sequence of $shP2X_4R$ was: 5′-GGG ATA AGA GAT ATA GGT AAC GTG TGC TGT CCG TTA CTT ATA TTT CTT GTC CCT TTT T-3′. We confirmed the specificity of P2×4R shRNAi by a coexpression assay. pCS-shP2×4R-CG was cotransfected into Cos7 cells with P2×4 expression plasmid (provided by Dr. K. Inoue) or HA-tagged P2Y12R plasmid (Supplemental information). pCS-shP2×4R-CG significantly suppressed P2×4R expression but had no effect P2Y12R expression. The recombined plasmid was cotransfected into 293FT cells (Invitrogen) with a packaging plasmid (pCAG-HIVgp) and a plasmid expressing Rev and vesicular stomatitis virus G glycoprotein (pCMV-VSV-G-RSV-Rev), and the supernatant was collected after 48 h and filtered through a 0.45-μm pore filter (Falcon). Viral particles in the supernatant were concentrated by ultracentrifugation for 2 h at 19,400 rpm (SW28 rotor; Beckmann Coulter, CA) and recovered by suspension in Hanks buffered saline (Invitrogen).

The recombinant lentivirus (2×10^5 infectious units) was added to the mixed glial cells that had been cultured for 12 days in a 25-cm^2 flask, and cultured for 6 days in DMEM containing 10% FCS. Floating cells were collected as microglia and allowed to attach to appropriate dishes or glasses. The efficiency of microglia transduction with the $shP2X_4R$ vector was 20–30%, the same as with the shControl vector according to an analysis of the number of microglia expressing EGFP by flow cytometry.

Isolation of EGFP-Positive Microglia

After transduction with the lentivirus vectors, floating cells collected as microglia were resuspended in PBS containing 2% FCS. EGFP-positive and -negative cells were sorted with a FACSVantageSE flow cytometry system (BD Biosciences). Live gating was performed with propidium iodide (Sigma-Aldrich, St. Louis, MO). The purity of the EGFP-positive cells was >99% according to a flow cytometry analysis.

Western Blot Analysis of P2X Receptor Expression

Sorted cells were lysed in SDS sample buffer. $P2X_4R$, $P2X_7R$, EGFP, and actin proteins in the lysate equivalent to 2×10^4 cells were separated by 10% SDS-PAGE and detected by Western blot analysis with 1 μg/mL anti-$P2X_4R$ antibody (Alomone Labs, Jerusalem, Israel), 0.6 μg/mL anti-$P2X_7R$ (Alomone Labs), anti-GFP antibody (diluted 1:1,000, Medical & Biological Laboratories, Nagoya, Japan), and anti-actin antibody (diluted 1:1,000, Sigma), respectively, and visualized with the ECL system.

RT-PCR Analysis for $P2Y_{12}R$ Gene Transcripts

RNA was isolated from the sorted cells with the RNeasy Mini Kit (QIAGEN, Hildem, Germany) containing a DNase treatment, according to the manufacturer's protocols. Reverse transcription of RNA was performed with SuperScript III reverse transcriptase (Invitrogen). The PCR amplification conditions were 30 s at 94°C, 15 s at 60°C, and 30 s at 68°C for 25–35 cycles, except for the initial denaturation step of 2 min at 94°C and the final cycle with an elongation step of 5 min at 68°C. An extra reaction mixture without reverse transcriptase was used as a control for DNA contamination of the RNA sample. The primers used were as follows: rat $P2Y_{12}R$, 5′-AAA CTT CCA GCC CCA GCA ATC T-3′ (forward), 5′-CAA GGC AGG CGT TCA AGG AC-3′ (reverse); rat β-actin, as an internal standard, 5′-TTG TTA CCA ACT GGG ACG ACA TGG-3′ (forward), 5′-GAT CTT GAT CTT CAT GGT GCT AGG-3′ (reverse). PCR products of 447 bp for $P2Y_{12}R$ and 763 bp for β-actin were analyzed on a 1.5% agarose and stained with ethidium bromide. The relative intensity of the bands for $P2Y_{12}R$ was quantified by densitometry with NIH image software and normalized to the β-actin products. The normalized values were used to calculate the ratio of $P2Y_{12}R$ mRNA level in the EGFP-positive cells transduced with the $shP2X_4R$ vector to the level in the EGFP-positive cells transduced with the shControl vector.

Calcium Imaging

The intracellular calcium concentration ($[Ca^{2+}]_i$) was monitored by the fura-2 method described by Inoue et al. (1998), using a highly sensitive intensifier target video camera C2400 and an Argus 50 image processor (Hama-

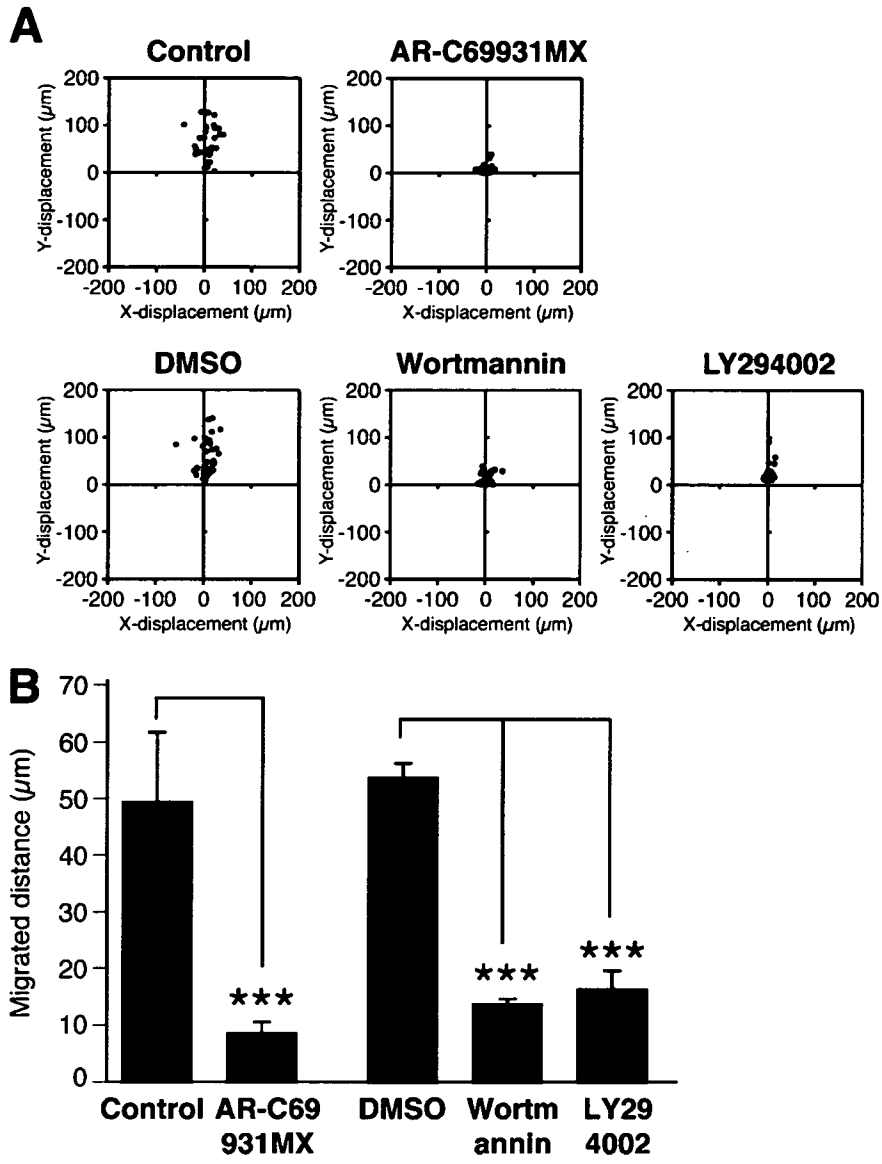

Fig. 1. Effect of PI3K inhibitors on ATP-induced microglial chemotaxis. (**A**) Microglia were pretreated with 1 μM AR-C69931MX for 10 min or with 0.125% DMSO, 100 nM wortmannin, or 50 μM LY294002 for 20 min, and microglial migration towards 50 μM ATP was observed in the Dunn chemotaxis chamber. The distance and direction migrated by individual cells are shown as x and y coordinates on scatter diagrams. The position of the outer well of the chamber is at the top in the vector diagrams of cells. (**B**) Chemotaxis by each cell was quantified by measuring the (x, y) distance migrated from the starting position. Data are means ± SD of three independent experiments. $^{***}P < 0.001$, Student's t-test.

matsu Photonics). Microglia transduced with the lentivirus vectors were plated at 2×10^5 cells/well on poly-L-lysine-coated CELLocate microgrid coverslips (Eppendorf, Hambrug, Germany). After 2 h, the cells were incubated with 10 μM fura-2 acetoxymethylester (fura-2/AM, Dojindo Laboratories, Kumamoto, Japan) at 37°C for 30 min in DMEM containing 25 mM HEPES (DMEM-H, Invitrogen), and the coverslips were mounted on an inverted epifluorescence microscope (TMD-300, Nikon, Tokyo, Japan). The cells were exposed to drugs dissolved in DMEM-H by superfusion. Raw data were recorded as 500-nm emissions of fura-2 excited alternately at 340 and 380 nm, and $[Ca^{2+}]_i$ was expressed as the ratio of the fluorescence intensity at 340 nm to the fluorescence intensity at 380 nm (F340/380).

RESULTS

Involvement of the PI3K Pathway in ATP-Induced Microglial Chemotaxis

We previously reported that ATP-induced microglial membrane ruffling were inhibited by treatment with pertussis toxin and a P2Y$_{12}$R-selective antagonist, AR-C69931MX, suggesting that Gi/o-coupled P2Y$_{12}$R is involved in both the membrane ruffling and the chemotaxis (Honda et al., 2001). Stimulation of P2Y$_{12}$R has been reported to induce PI3K activation (Czajkowski et al., 2004; Soulet et al., 2004; Van Kolen and Slegers, 2004). To determine whether PI3K activation is required for chemotaxis by ATP-stimulated microglia, we investigated the effects of the PI3K inhibitors wortmannin and

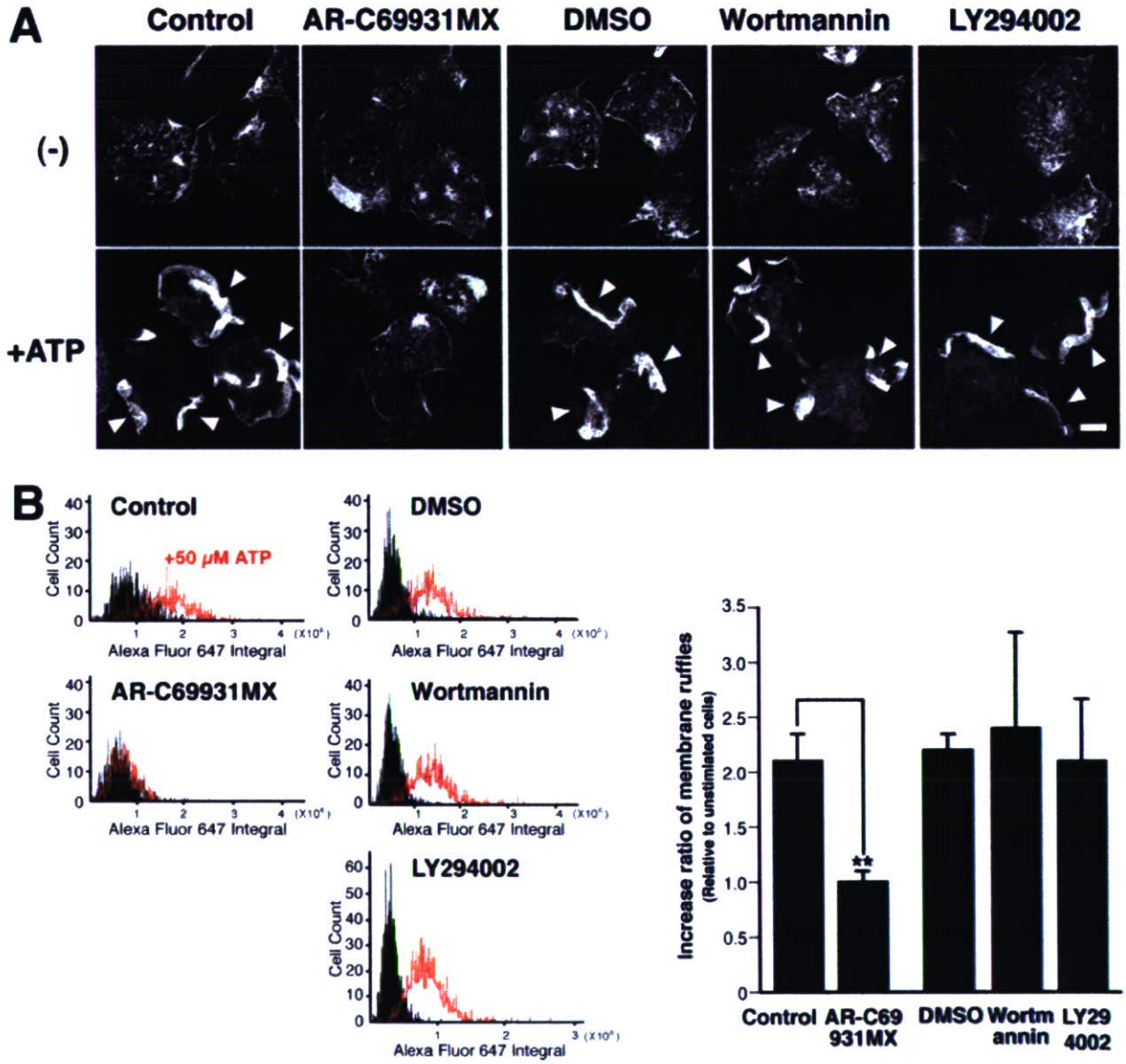

Fig. 2. Effect of PI3K inhibitors on ATP-induced microglial membrane ruffling. (**A**) Microglia were pretreated with 1 μM AR-C69931MX, 0.125% DMSO, 100 nM wortmannin, or 50 μM LY294002 as described in Fig. 1A, and then stimulated with 50 μM ATP for 5 min. After fixation, the cells were stained with Texas Red-conjugated phalloidin to visualize membrane ruffles. Arrowheads indicate membrane ruffles. Scale bar, 10 μm. (**B**) Quantification of membrane ruffles. Microglia were stimulated as in A for 5 min, fixed, and stained with an anti-Iba1 antibody and Alexa Fluor 647-conjugated phalloidin to recognize individual microglial cells and membrane ruffles, respectively. The F-actin content of microglial cells was quantified as integral intensity of Alexa Fluor 647 fluorescence by using LSC. The five panels on the left side are histograms representing the total F-actin in each cell (*x*-axis, Alexa fluor 647 integral) and the number of scanned cells (*y*-axis, cell count). The black region represents the unstimulated cells, and the region surrounded by the red line represents the ATP-stimulated cells. The bar graph on the right side shows the ratio of the mean of fluorescent intensity of ATP-stimulated cells to that of unstimulated cells after treatment with each inhibitor. Data are means ± SD of three independent experiments. $^{**}P < 0.01$, Student's *t*-test.

LY294002 with a Dunn chemotaxis chamber. Microglial chemotaxis toward the higher concentration of ATP was evaluated by analysis of time-lapse images. When 50 μM ATP was applied to the outer well, the cells migrated toward higher concentrations of ATP. Pretreatment of the microglia with wortmannin or LY294002 significantly blocked the chemotaxis (Fig. 1A). The chemotactic movement of the microglia was quantified by calculating the (x, y) distances individual cells migrated toward ATP. As shown in Fig. 1B, the mean distance migrated by cells pretreated with PI3K inhibitors was significantly shorter than the distance migrated by cells pretreated with DMSO. Treatment with 1 μM AR-C69931MX also inhibited the chemotaxis, as expected based on the results of our previous study (Honda et al., 2001). These findings suggested that PI3K activation is necessary for ATP-induced microglial chemotaxis.